

Embracing Unknown Step by Step: Towards Reliable Sparse Training in Real World

Bowen Lei

*Department of Statistics
Texas A&M University*

bowenlei@stat.tamu.edu

Dongkuan Xu

*Department of Computer Science
North Carolina State University*

dxu27@ncsu.edu

Ruqi Zhang

*Department of Computer Science
Purdue University*

ruqiz@purdue.edu

Bani Mallick

*Department of Statistics
Texas A&M University*

bmallick@stat.tamu.edu

Reviewed on OpenReview: <https://openreview.net/forum?id=Db5c3Wxj9E>

Abstract

Sparse training has emerged as a promising method for resource-efficient deep neural networks (DNNs) in real-world applications. However, the reliability of sparse models remains a crucial concern, particularly in detecting unknown out-of-distribution (OOD) data. This study addresses the knowledge gap by investigating the reliability of sparse training from an OOD perspective and reveals that sparse training exacerbates OOD unreliability. The lack of unknown information and the sparse constraints hinder the effective exploration of weight space and accurate differentiation between known and unknown knowledge. To tackle these challenges, we propose a new unknown-aware sparse training method, which incorporates a loss modification, auto-tuning strategy, and a voting scheme to guide weight space exploration and mitigate confusion between known and unknown information without incurring significant additional costs or requiring access to additional OOD data. Theoretical insights demonstrate how our method reduces model confidence when faced with OOD samples. Empirical experiments across multiple datasets, model architectures, and sparsity levels validate the effectiveness of our method, with improvements of up to **8.4%** in AUROC while maintaining comparable or higher accuracy and calibration. This research enhances the understanding and readiness of sparse DNNs for deployment in resource-limited applications. Our code is available on: <https://github.com/StevenBoys/MOON>.

1 Introduction

Sparse training is one popular method for achieving resource efficiency in deep neural networks (DNNs), and it is receiving growing attention when considering the resource-limited real-world applications of DNNs (Bellec et al., 2017; Evci et al., 2020; Yuan et al., 2021). By maintaining sparse weights throughout the training process, sparse training accelerates the training of DNNs, saves training memory, and produces sparse models with dense performance levels (Mocanu et al., 2018; Dettmers & Zettlemoyer, 2019; Evci et al., 2020; Liu et al., 2022a), which has been applied to an increasing number of tasks (Yuan et al., 2021; Sokar et al., 2021; Bibikar et al., 2022). There remains, however, a critical question that needs to be answered before sparse

arXiv:2403.20047v1 [cs.LG] 29 Mar 2024

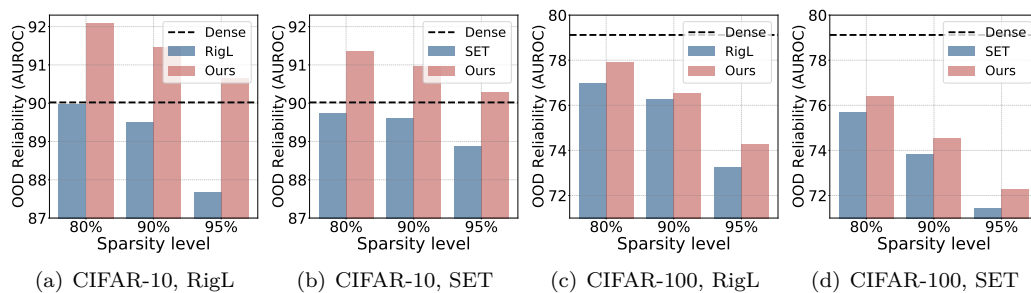


Figure 1: OOD reliability (measured by AUROC (%), the higher the better) of the ResNet-18 produced by dense and sparse training (RigL & SET) on CIFAR-10/100. Compared to dense training (black line), sparse training (blue bar) has a smaller AUROC, indicating sparse training exacerbates the unreliability on OOD data. Our MOON (red bar) improves AUROC and OOD detection.

training can be safely introduced in real-world applications: how reliable the sparse model is in the real world?

Reliable models in real-world scenarios possess the ability to recognize situations in which they are likely to be wrong, such as identifying unknown OOD data, and refrain from providing incorrect responses (Wang et al., 2021b; Vaze et al., 2021; Du et al., 2022). However, the investigation of OOD detection within the context of sparse training remains unexplored, creating an important knowledge gap that hinders a comprehensive assessment of the readiness of DNNs for deployment. Models with weak OOD detection are prone to feign understanding and provide arbitrary guesses on unrecognizable OOD data, leading to safety concerns (Liu et al., 2020; Hsu et al., 2020; Du et al., 2022; Wang et al., 2021b) in scenarios, e.g., automated healthcare and self-driving cars (Rasheed et al., 2022; De Silva & Mycroft, 2022).

In this work, we investigate for the *first* time the reliability of sparse training from the OOD perspective, and find that sparse training exacerbates the OOD unreliability. Figure 1 compares AUROC (i.e., a metric for OOD detection, the higher the better) (Yang et al., 2022) between dense and sparse training, e.g., RigL (Evcı et al., 2020) and SET (Mocanu et al., 2018). The AUROC is smaller for sparse training (blue bar) compared to dense training (black line), indicating that sparse training weakens the OOD detection capacity. In order to address the OOD unreliability of sparse training, we raise the following questions:

Question 1. *Why sparse training exacerbates the OOD unreliability in DNNs?*

The underlying determinant of weak OOD detection is the lack of unknown information, and sparse constraints hinder the effective communication of unknown concepts with DNNs. In order to recognize OOD samples, the model needs to distinguish between the known and the unknown. However, it has been shown that DNNs tend to focus on the known due to the close nature of the training process and ignore the rest (Bendale & Boulton, 2016; Padhy et al., 2020; Wang et al., 2021b). There are studies trying to encourage DNNs to learn more about the unknown. But they usually focus on dense training. When moving to sparse training, the sparsity cuts off update routes and produces spurious local minima (Evcı et al., 2019; Sun & Li, 2021; He et al., 2022), which makes the exploration of the weight space more challenging, and thus more difficult to search for and find reliable models (Lei et al., 2023b). Thus, the sparse training exacerbates the OOD unreliability in DNNs.

Question 2. *How can we leverage unknown information under sparse constraints to effectively guide weight space exploration to OOD-reliable state?*

To improve OOD reliability, it is crucial to utilize unknown information to guide model training. The sparsity constraint increases the difficulty of exploring the weight space and prevents the unknown information from guiding the model training to an OOD-reliable state. Efforts have been made to exploit unknown information in dense DNNs (Thulasidasan et al., 2019; Wang et al., 2021b; Roy et al., 2022). However, DAC (Thulasidasan et al., 2019) is limited to the treatment to label noise and lacks a comprehensive guide to OOD detection. EOW-Softmax (Wang et al., 2021b) only indirectly and inadequately exploits the unknown and incurs considerable additional costs. Moreover, HOD (Roy et al., 2022) require access to OOD data, which is often a non-trivial task. To address these issues and adapt to the challenges in sparse training, we propose a new outlier-exposure-free training loss that extracts unknown information from hard ID samples and then directly tells the DNNs this unknown information, which gives an effective guide for weight space exploration under sparse constraints with only a slight increase in computational and storage burden.

Question 3. *How can we address the confusion between known and unknown information in sparse training to avoid providing misleading guidance for weight space exploration?*

Despite the possibility of communicating unknown information, sparse DNNs are more likely to confuse known and unknown information, resulting in poor performance and reliability. DNNs show performance degradation in sparse training with high sparsity (Mocanu et al., 2018; Evci et al., 2020; Lei et al., 2023b), especially in the early training stage, which indicates the challenge of understanding knowable content under sparsity constraints. Therefore, to avoid confusion and provide proper guidance for training, we also design an auto-tuning strategy that allows the DNN to mainly discover the known in the early stage and embrace the unknown in the later stage step by step. In addition, we propose a voting scheme that combines information from multiple models for a more comprehensive understanding of the known and unknown.

In summary, our contributions are summarized as follows:

- We for the first time investigate how sparse training influences OOD reliability and analyze the hidden reasons. We find that sparse training exacerbates the OOD unreliability of DNNs.
- We propose a new model-agnostic unknown-aware sparse training method (MOON) to improve real-world reliability, which allows the model to be aware of what it does not know via a loss modification, auto-tuning strategy, and a voting scheme at little additional cost.
- We provide theoretical insights on how our MOON method reduces the confidence of the model when faced with OOD samples and improves OOD reliability.
- Empirically, we conduct extensive experiments on multiple benchmark datasets, model architectures, and sparsity. Our MOON improves the AUROC by up to **8.4%** and successfully upholds the accuracy, calibration, and other pertinent metrics associated with sparse training, thereby complementing existing research and further enhancing the efficacy and applicability of the sparse training paradigm.

2 Related Work

Sparse Training. As models continue to grow in size, there is an increasing focus on sparse training, where sparse weights are maintained during training to accommodate resource-limited real-world deployments (Mocanu et al., 2018; Bellec et al., 2018; Huang et al., 2023). To find a sparse model with good performance, the sparse topology is updated by pruning and growth steps after every fixed number of iterations (Evci et al., 2020; Huang et al., 2022). A variety of sparse training methods have been investigated and various pruning and growth criteria, such as weights and gradient magnitude, have been developed (Mostafa & Wang, 2019; Dettmers & Zettlemoyer, 2019; Evci et al., 2020; Jayakumar et al., 2020; Liu et al., 2021b; Özdenizci & Legenstein, 2021; Zhou et al., 2021; Schwarz et al., 2021; Yin et al., 2022; Lei et al., 2023a). Existing work mainly targets saving more resources and at the same time maintaining accuracy. However, despite saving resources, sparse training can result in more difficult training due to the cut-off update routes and the generation of spurious local minima, raising safety concerns on both ID and OOD data.

Confidence Calibration. DNNs’ reliability on ID data is increasingly important, which usually refers to whether the confidence of DNNs on ID data is well calibrated (Guo et al., 2017; Nixon et al., 2019; Zhang et al., 2020; Wu et al., 2023). Prior work has shown that DNNs tend to be over-confident (Guo et al., 2017; Rahaman et al., 2021; Patel et al., 2022; Zhu et al., 2023), misleading humans and raising safety concerns. Research has been conducted to improve confidence calibration, where widely-used methods include temperature scaling (Guo et al., 2017), Mixup (Zhang et al., 2017), label smoothing (Szegedy et al., 2016), and Bayesian methods (Gal & Ghahramani, 2016; Ashukha et al., 2020). Recently, ID reliability in sparse training has also been studied in Sup-tickets (Yin et al., 2022) and CigL (Lei et al., 2023b).

OOD Detection & Open-set Classification. For real-world tasks, reliability on OOD data, i.e., OOD detection capability, is also critical due to the presence of unknown categories. It is also referred to as open-set classification when ID classification is required as well (Yang et al., 2021b; Vaze et al., 2021). When these unknown categories are given, a reliable model should detect them and refuse to answer, rather than giving random guesses. Research has been devoted to OOD detection, including post-processing methods (Hendrycks

& Gimpel, 2016; Liang et al., 2017; Liu et al., 2020), training time regularization (DeVries & Taylor, 2018; Hsu et al., 2020; Du et al., 2022), and training with outlier exposure (Hendrycks et al., 2018; Yu & Aizawa, 2019; Yang et al., 2021a). However, existing OOD reliability studies have mainly focused on dense training and have not yet fully explored sparse training settings.

OOD reliability of sparse DNNs. Despite the lack of exploration of sparse training, there are studies on the OOD reliability of sparse DNNs. The effect of random pruning on the sparse DNNs with fixed sparsity patterns is studied (Liu et al., 2022b), while sparse training has dynamic sparsity patterns that provide better performance compared to fixed patterns. It is also investigated how to obtain deep ensembles that outperform dense models through sparse training, which requires a non-trivial additional cost (Liu et al., 2021a). Thus, generating a single sparse network through sparse training remains irreplaceable when resources are limited. In addition, efforts have been devoted to OOD reliability of pruning methods, which start with a dense model and gradually prune the weights, reducing the difficulty of exploring the weight space (Ayle et al., 2022; Cheng et al., 2023). In contrast, sparse training maintains a high level of sparsity throughout the training process, which cuts off a large portion of the route and produces more spurious local minima, thus making weight space exploration more challenging and having different properties from pruning methods (Chen et al., 2022b).

Extra Dimension. Adding an extra dimension to the output of the K -way classification model has been studied and used to relax closed-world setting to open-world setting (Hsu et al., 2020; Mozannar & Sontag, 2020; Wang et al., 2021b; Verma & Nalisnick, 2022; Liu et al., 2023). Specifically, the close-world setting assumes the test data has the same distribution as the training data, which is not always true in the real world. The open-world setting, on the other hand, allows for unknown classes in the test data. Previous work has used extra dimension to abstain from making decisions on noisy labels (Thulasidasan et al., 2019) or to improve OOD detection in dense DNNs (Wang et al., 2021b; Roy et al., 2022). However, they do not directly exploit the unknown information and incur extra costs (Wang et al., 2021b), or require exposure to OOD data (Roy et al., 2022). In addition, they all ignore how to add extra dimensions in sparse training.

3 Method

We propose a new sparse training method MOON to improve the real-world reliability of DNNs, i.e., to provide effective detection for OOD data under sparsity constraints with comparable or higher ID accuracy and reliability. Importantly, MOON can be seamlessly integrated as a plug-in method and combined with existing OOD detection methods. Specifically, we add an extra dimension in the output probability and propose a new unknown-aware loss with an auto-tuning strategy to gradually encourage DNNs to consider more unknown information. Then, we combine information from multiple models into the output model via a voting scheme so that the output model has a comprehensive view of what is known and what is unknown, providing reliable predictions.

3.1 Tell Model What It Doesn't Know

In general, given the data $\{x_i, y_i\}_{i=1}^N$ where $y \in \{1, \dots, K\}$, the model is forced to classify new input data into K predefined classes by the widely used cross-entropy loss, even if the model is uncertain about the class of the samples or has never seen this class before (Wang et al., 2021b). We argue that ignorance of unknown information during weight space exploration, i.e., the sample for which the model gives incorrect predictions ($\hat{y}_i \neq y_i$), is the cause of this unreliability. Sparse constraints further make the exploration more challenging and thus require better guidance from unknown information. To solve these problems, we utilize $K+1$ -way formulation and propose a new unknown-aware loss to tell the model what is unknown to it during sparse training. Unlike existing methods, we directly tell DNNs the unknown, providing an effective guide to cope with the challenges posed by sparsity.

$K+1$ -way formulation: To store the unknown information, inspired by previous work on dense DNNs with extra dimensions (Thulasidasan et al., 2019; Wang et al., 2021b; Roy et al., 2022), we add an extra dimension in the softmax formulation, allowing the model to provide a $K + 1$ -dimensional output probability $f(x_i) = (p_1, \dots, p_K, p_{K+1})$ for each x_i , unlike the previous K -way formulation. The first K dimensions

(p_1, \dots, p_K) represent the model’s beliefs about class attribution, while the $K + 1$ -th dimension p_{K+1} is designed to store unknown information. Ideally, the model gives larger probabilities for the true class dimension p_{y_i} when the model knows the input samples very well. Otherwise, the model provides larger p_{K+1} and smaller (p_1, \dots, p_K) to avoid unreliable random guesses in the K classes.

Unknown-aware Loss Modification: To incorporate unknown information into the model, we design an unknown-aware loss shown in Eq. (1). On the one hand, when the model knows the sample x_i well and makes correct predictions (i.e., $\hat{y}_i = y_i$), we choose the broadly-used cross-entropy loss for x_i to encourage larger p_{y_i} . On the other hand, if the model does not have enough understanding of harder sample x_i and makes wrong predictions (i.e., $\hat{y}_i \neq y_i$), we use a new-designed loss to increase reliability. Specifically, in the new loss, we add a larger weight $(1 + \frac{w}{1+wp_{K+1}})$ to encourage the model to focus more on the samples it predicts incorrectly. To reduce the loss, the model can determine the correct class (i.e., give a larger p_{y_i}) or provide a larger p_{K+1} such that (p_1, \dots, p_K) becomes smaller, indicating that the model is uncertain about its prediction.

$$L(x_i) = \begin{cases} -\log p_{y_i} & \hat{y}_i = y_i \\ -(1 + \frac{w}{1+wp_{K+1}}) \log p_{y_i} & \hat{y}_i \neq y_i \end{cases} \quad (1)$$

3.2 Do not Frustrate Model in Early Stage

We find that telling the model too much about the unknowns at the beginning can lead to more severe unreliability (see Section 5.7), especially in cases where the weight space is insufficiently explored (e.g., highly sparse models). It is as if too much emphasis on unknowns frustrates the model and prevents it from finding out what it can know. Thus, inspired by (Thulasidasan et al., 2019), we design an auto-tuning strategy for w in the unknown-aware loss (i.e., Eq. (1)) to step-by-step inform the model about the unknown information, which is outlined in Algorithm 1. In this way, p_{y_i} and p_{K+1} can better help the model learn and store both the known and unknown information.

In the early stage (i.e., epoch $t \leq T_e$), we fix w to zero so that the new loss is equivalent to the cross-entropy loss and no unknown information is emphasized. DNNs usually learn easy samples in the early stage of training and tend to fit the hard ones later (Wang et al., 2021a). Thus, in the beginning, the model does not learn the data well and usually makes many wrong predictions. With insufficient exploration of the weight space, a large w will unnecessarily put more emphasis on harder samples and prevent the model from learning easy samples, leading to poor reliability. The model is like a new learner, and it is advisable not to point out its mistakes too much, in case it gets frustrated.

After the early stage (i.e., epoch $t > T_e$), we start telling the model what is unknown. We keep w as a constant at each epoch and increase it from the initial value w_i to the final value w_f after each epoch via a linear scheduler. **The initial** w_i is based on the $\beta = (1 - p_{K+1})L(x_i)$ and calculated in the early stage. On the one hand, if we get smaller p_{K+1} and larger $L(x_i)$, we can know that the model hasn’t learned the data well while it is over-confident about its wrong predictions. Thus, we will set a larger β and w_i , in this case, to emphasize more on the unknown for reliability. On the other hand, if we get larger p_{K+1} and smaller $L(x_i)$, we can know that the model learns the data well and is cautious about its output. Therefore, we can encourage the model to find out more about what it can know with smaller β and w_i . For the initial factor r , it is used to control the initial value

Algorithm 1: w Auto-tuning Scheduler

Input: Total epoch T , current epoch t , unknown-free epoch T_e , probability $\{p_i\}_{i=1}^{K+1}$, unknown-free loss L , init factor r , final weight w_f , smoothing factor α .

Output: The weight w for the unknown-aware loss.

Initialization:

$w = 0$, $\tilde{\beta} = 0$, and $\delta = -1$

if $t < T_e$ **then**

 Prepare information for the initial weight:

$\beta = (1 - p_{K+1})L(x_i)$

 Use moving average $\tilde{\beta} = (1 - \alpha)\tilde{\beta} + \alpha\beta$

else if $\delta = -1$ **then**

 Calculate the initial weight $w_i = \frac{\tilde{\beta}}{r}$ and $w = w_i$

 Calculate the step size $\delta = \frac{w_f - w_i}{T - T_e}$ of the scheduler

else

 Calculate weight at epoch t :

$w = w_i + (t - T_e) \cdot \delta$

end

w_i to avoid w being too large. **For the final** w_f , it is a pre-determined hyper-parameter, which is usually larger than w_i . At each epoch after T_e , we set a linear increase scheduler $w = w_i + (t - T_e) \cdot \delta$ where the step size $\delta = (w_f - w_i)/(T - T_e)$, allowing more attention on the unknown at the later stage of the training.

3.3 Vote for Known and Unknown: Weight Averaging

We further design a voting strategy that combines information from multiple models to give the output model a more comprehensive sense of what it knows and what it does not know. Specifically, at the end of the proposed unknown-aware training (e.g., after 80% training epochs), we collect models at each epoch and use the weight averaging method (Izmailov et al., 2018; Wortsman et al., 2022) to uniformly average them into one output model. In this way, we let multiple models decide what is known and unknown together, allowing a fuller understanding of the learned knowledge and more reliable predictions.

4 Theoretical Insight

We provide a couple of theoretical insights to demonstrate that our model-agnostic unknown-aware sparse training method MOON can produce more reliable predictions in the face of out-of-distribution (OOD) data. The unknown information is extracted from hard in-distribution (ID) data, which explains the outlier-exposure-free property of MOON. Detailed proofs are presented in the Appendix. Without loss of generality, suppose the goal is a two-way classification based on $\{x_i, y_i\}_{i=1}^N$ where $y_i \in \{1, 2\}$. We have a deep neural network $f = g \circ h$, which can be seen as a composition of feature mapping function h and the softmax classification function g .

We first show how we can extract the unknown from the hard ID data. The following analysis is based on Assumption 4.1, which has been widely used in several studies of OOD detection (Lee et al., 2018; Ahuja et al., 2019; Morteza & Li, 2022).

Assumption 4.1. (Gaussian Mixture Feature Space): The feature mapping function h maps the input ID data to a Gaussian mixture $v_1\mathcal{N}(\mu_1, \Sigma_1) + v_2\mathcal{N}(\mu_2, \Sigma_2)$. Specifically, when $y = 1$, we have $h(x) \sim \mathcal{N}(\mu_1, \Sigma_1)$. And when $y = 2$, we have $h(x) \sim \mathcal{N}(\mu_2, \Sigma_2)$.

We define the definition of unreliability for a set of ID data.

Definition 4.2. (Unreliability) For samples whose features are around $h(x_0)$, i.e., $D(\epsilon_0) = \{(x, y); \|h(x) - h(x_0)\| < \epsilon_0\}$, the predictions are unreliable around x_0 if for any $0 < \epsilon < \epsilon_0$, we can find $\eta > 0$ such that

$$\mathbf{E}_{D(\epsilon)}[\max_{c \in \{1, 2\}} \mathcal{N}(h(x); \mu_c, \Sigma_c)] - \mathbf{E}_{D(\epsilon)}[1\{\hat{y} = y\}] > \eta. \quad (2)$$

Remark 4.3. Definition 4.2 gives a mathematical expression for the ID unreliability in feature space (i.e., the discrepancy between confidence and accuracy) around $h(x_0)$. The first term $\mathbf{E}_{D(\epsilon)}[\max_{c \in \{1, 2\}} \mathcal{N}(x; \mu_c, \Sigma_c)]$ denotes the expected confidence around $h(x_0)$, and the second term $\mathbf{E}_{D(\epsilon)}[1\{\hat{y} = y\}]$ refers to the expected accuracy. For a threshold (e.g., η), we consider predictions to be unreliable if the discrepancy between confidence and accuracy cannot be reduced below η no matter how we alter ϵ . This extends the definition of unreliability from the global aspect to the local region around $h(x_0)$ in feature space and helps to describe unreliability within hard samples.

Insight 4.4. (Unreliability) Suppose we have (x_1, y_1) from class 1 and $D_2 = \{(x, y); \|h(x) - h(x_1)\| < \epsilon, y = 2\}$ from class 2. Then, unreliability can occur around $h(x_1)$.

Remark 4.5. The setting in Insight 4.4 is common for the hard ID samples, resulting in unreliability. Samples with large feature differences within two classes are easy to classify, with both high accuracy and confidence. While samples with minor differences can puzzle the model, with low accuracy and high confidence, resulting in over-confidence.

Insight 4.6. (Hard-ID Reliability) Suppose we have the same (x_1, y_1) and D_2 as in Insight 4.4. If the model is trained with our MOON method and the extra dimension successfully stores the unknown information, the unreliability can be solved, i.e., for any $\eta > 0$, we can find $0 < \epsilon < \epsilon_0$ such that

$$\mathbf{E}_{D(\epsilon)}[\max_{c \in \{1, 2\}} \mathcal{N}(h(x); \mu_c, \Sigma_c)] - \mathbf{E}_{D(\epsilon)}[1\{\hat{y} = y\}] < \eta. \quad (3)$$

Remark 4.7. Insight 4.6 shows that our MOON method reduces the confidence level and decreases the discrepancy, solving the unreliability issue when the model is faced with some hard ID samples.

We further show how OOD detection can benefit from the unknown information from hard ID data.

Insight 4.8. (OOD Reliability) Suppose we achieve Hard-ID Reliability in Insight 4.6 with our MOON method, we can have lower confidence on OOD data, implying stronger OOD detection.

Remark 4.9. Insight 4.8 show that OOD detection can be enhanced by the unknown information extracted from the hard ID data. Existing work has found that ID data contain information for the OOD samples (Du et al., 2022). It is found that ID samples from the low-likelihood region of the class-conditional distribution, i.e., hard-to-detect ID data, are similar to OOD samples in the feature space, which is similar to the scenario described in Insight 4.4. Although we do not use OOD data in the training, these hard-to-detect ID samples can be viewed as pseudo-OOD data. With our MOON method, the model knows which hard ID samples it does not know and provides lower confidence for these samples (i.e., pseudo-OOD data). Since the real OOD data are neighbors of the pseudo-OOD data in the feature space, the model also gives a low confidence for the real OOD data.

5 Experiments

We perform a comprehensive empirical evaluation of our MOON , where we add our MOON to the training of multiple benchmark datasets, model architectures, and sparsities, and compare it with the original sparse training results.

Datasets & Model Architectures: For in-distribution (ID) data, we include four benchmark datasets: MNIST (Deng, 2012), CIFAR-10 and CIFAR-100 (Krizhevsky et al., 2009) and ImageNet-2012 (Russakovsky et al., 2015). For out-of-distribution (OOD) data, we follow the setups of OpenOOD (Yang et al., 2022) (more details in Appendix B.1). For model architectures, we choose ResNet-18 to train MNIST, CIFAR-10, and CIFAR-100, and choose ResNet-50 to train ImageNet-2012 (He et al., 2016). We repeat all experiments 3 times and calculate the mean and standard deviation.

Training Settings: For sparse training, we study two widely-used methods, e.g., RigL (Evci et al., 2020) and SET (Mocanu et al., 2018), and a variety of sparsities, including 80%, 90%, 95%, and 99%, which sufficiently reduces the cost and is of great interest in real-world deployments. We also examine the performance of dense training to show the broad applicability of our method (see Appendix A.3).

Implementations: We follow the settings of OpenOOD (Yang et al., 2022). We choose SGD with momentum and use the cosine annealing learning rate scheduler. We train all the models for 100 epochs. For the batch size, we set it to 128 in MNIST, CIFAR-10, and CIFAR-100, and 32 in ImageNet.

Comparison Metrics: To measure OOD detection capability, we chose AUROC and FPR-95 (Yang et al., 2022). For AUROC, it calculates the area under the receiver operating characteristic (ROC) curve, where a larger AUROC suggests better OOD detection. For FPR-95, it measures the false positive rate (FPR) at a true positive rate (TPR) of 95%, where a lower FPR-95 implies better OOD detection. To compare ID reliability, we choose ECE (Guo et al., 2017) and test accuracy. ECE measures the discrepancy between confidence and true accuracy, with lower ECE indicating higher ID reliability.

5.1 OOD Detection in Sparse Training

In this section, we show that our MOON can improve OOD detection in sparse training, including 80%, 90%, 95%, and 99% sparsities using RigL. Since our MOON requires no additional OOD data and training, to fairly compare the OOD reliability, we incorporate our MOON into the widely-used post-process OOD detection methods MSP (Hendrycks & Gimpel, 2016) and compare the results MSP.

For CIFAR-10 based models, we examine its OOD detection capacity on two near OOD data, i.e., CIFAR-100 (Chandola et al., 2009) and TIN (Han et al., 2022)), and four far OOD data, i.e., MNIST (Deng, 2012), SVHN (Netzer et al., 2011), Texture (Ahmed & Courville, 2020), Places365 (Guo et al., 2017). As shown in Table 1, the columns named “NearOOD” and “FarOOD” represent the average detection scores

Table 1: Comparison of OOD detection by AUROC (%) (\uparrow) between MOON +MSP (*M-MSP*) and MSP for CIFAR-10 in sparse training. Our MOON leads to larger AUROC on each OOD data of CIFAR-10, showing its ability to improve reliability on OOD data.

		CIFAR-100	TIN	NEAROOD	MNIST	SVHN	TEXTURE	PLACES365	FAROOD
80%	MSP	87.43 (0.2)	88.92 (0.2)	88.17 (0.2)	92.92 (0.8)	91.81 (0.7)	89.35 (0.3)	89.44 (0.2)	90.88 (0.5)
	<i>M-MSP</i>	89.93 (0.1)	91.14 (0.1)	90.53 (0.1)	95.00 (0.7)	93.82 (0.5)	91.80 (0.2)	90.82 (0.3)	92.86 (0.4)
90%	MSP	87.78 (0.2)	89.12 (0.1)	88.45 (0.1)	91.82 (0.9)	91.48 (0.5)	87.90 (0.3)	88.93 (0.2)	90.03 (0.4)
	<i>M-MSP</i>	88.92 (0.2)	90.34 (0.2)	89.63 (0.2)	95.39 (0.8)	93.09 (0.4)	91.09 (0.4)	89.92 (0.2)	92.37 (0.4)
95%	MSP	86.04 (0.1)	87.30 (0.1)	86.67 (0.1)	93.74 (0.6)	86.09 (0.8)	85.26 (0.3)	87.68 (0.2)	88.19 (0.5)
	<i>M-MSP</i>	88.04 (0.1)	89.39 (0.2)	88.71 (0.1)	94.76 (0.7)	93.35 (0.8)	89.86 (0.3)	88.51 (0.3)	91.62 (0.5)
99%	MSP	80.94 (0.2)	82.75 (0.2)	81.84 (0.2)	88.34 (0.8)	85.75 (0.7)	83.43 (0.2)	80.45 (0.2)	84.49 (0.5)
	<i>M-MSP</i>	83.75 (0.1)	85.11 (0.1)	84.43 (0.1)	91.96 (0.8)	89.01 (0.8)	86.44 (0.3)	83.38 (0.2)	87.70 (0.5)

of the near OOD data and the far OOD data, respectively. As shown in Table 1, the AUROC value drops with increasing sparsity, which implies the unreliability issues in sparse training. Our MOON obtains a larger AUROC on each OOD data of CIFAR-10, where the improvement of AUROC can be up to 8.4%. This indicates MOON’s ability to improve the reliability on OOD data in sparse training.

For the model trained on ImageNet-2012, we examine its OOD detection ability on four near OOD data, i.e., Species (SP) (Torralla et al., 2008), iNaturalist (IN) (Shorten & Khoshgoftaar, 2019), OpenImage-O (OO) (Li et al., 2021), ImageNet-O (IO) (Sun et al., 2022), and two far OOD data, i.e., Texture (TX) (Ahmed & Courville, 2020), MNIST (MN) (Deng, 2012). As shown in Figure 2, the red and blue bars represent our MOON and MSP, respectively. We can see that our MOON provides larger AUROC and smaller FPR-95 almost on all of the OOD data of ImageNet-2012, showing its effective OOD detection in sparse training.

To show the general applicability of our method, we also incorporate our MOON into other broadly-used post-processing OOD detection methods, e.g., ODIN (Liang et al., 2017), EBO (Liu et al., 2020), KNN (Sun et al., 2022), and KLM (Hendrycks et al., 2022), and compare the results with those using only ODIN and EBO. We take sparse models on CIFAR-10 using RigL as an example. First, we consider 99% sparsity while considering ODIN and EBO as baselines. As shown in Table 2, our MOON leads to larger AUROC and smaller FPR-95 on each OOD data compared to ODIN and EBO. Then, for KNN and KLM, we also experiment on different sparsity levels including 80%, 90%, 95%, and 99%. As shown in Table 3, our MOON leads to a larger AUROC on each OOD data compared to KNN and KLM. This shows that the ability of our MOON to improve OOD reliability is consistent under sparsity constraints for different OOD detection methods.

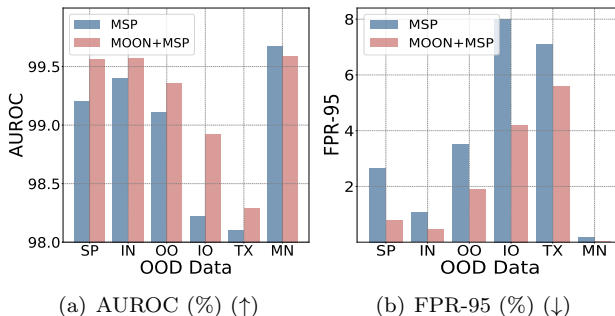


Figure 2: Comparison of OOD detection by AUROC (%) (\uparrow) and FPR-95 (%) (\downarrow) between MOON +MSP and MSP for ImageNet-2012 using RigL (90%). MOON leads to larger AUROC and smaller FPR-95 on OOD data of ImageNet-2012, showing improved OOD reliability in sparse training.

5.2 Comparison with Calibration Method

Prior work shows that calibration methods can help with OOD detection in dense DNNs (Wang et al., 2021b; Yang et al., 2022). To show the ineffectiveness of existing calibration methods for OOD detection in sparse training, we also compare our MOON to calibration methods including temperature scaling (Lee et al., 2018), Mixup (Zhang et al., 2017), and CigL (Lei et al., 2023b) using RigL (90%) for OOD detection capability. For our MOON, we report the results of “MOON + ODIN”. As shown in Figure 3, the red and blue hexagons

Table 2: Comparison of OOD detection by AUROC (%) (\uparrow) & FPR-95 (%) (\downarrow) between MOON +ODIN (*M-ODIN*), MOON +EBO (*M-EBO*) and baseline post process methods (i.e., ODIN and EBO) for CIFAR-10 using RigL (99% sparsity). Our MOON leads to larger AUROC and smaller FPR-95 on each OOD data, showing its ability to improve reliability on OOD data in sparse training.

		CIFAR-100	TIN	NEAROOD	MNIST	SVHN	TEXTURE	PLACES365	FAROOD
AUROC	ODIN	84.09 (0.2)	86.98 (0.3)	85.54 (0.2)	96.82 (0.5)	89.11 (0.7)	87.47 (0.3)	85.49 (0.2)	89.72 (0.4)
	<i>M-ODIN</i>	90.59 (0.3)	92.64 (0.2)	91.61 (0.2)	99.21 (0.7)	93.91 (0.8)	93.26 (0.2)	93.35 (0.2)	94.93 (0.5)
	EBO	83.73 (0.3)	86.93 (0.3)	85.33 (0.3)	94.68 (0.6)	85.71 (0.5)	85.09 (0.2)	85.44 (0.2)	87.73 (0.4)
	<i>M-EBO</i>	85.64 (0.2)	88.55 (0.3)	87.09 (0.2)	97.10 (0.7)	87.35 (0.4)	87.11 (0.3)	88.55 (0.3)	90.03 (0.4)
FPR-95	ODIN	67.99 (0.8)	61.54 (0.5)	64.76 (0.6)	19.40 (1.6)	65.32 (1.7)	56.58 (0.6)	62.56 (0.7)	50.97 (1.1)
	<i>M-ODIN</i>	61.23 (0.8)	56.00 (0.6)	58.62 (0.7)	11.58 (1.8)	57.67 (2.1)	51.81 (0.5)	54.09 (0.7)	43.79 (1.3)
	EBO	69.42 (0.7)	61.15 (0.6)	65.29 (0.6)	34.49 (1.4)	78.09 (1.2)	67.64 (0.6)	61.23 (0.7)	60.36 (1.0)
	<i>M-EBO</i>	63.30 (0.7)	55.85 (0.5)	59.58 (0.6)	16.37 (1.6)	77.70 (0.7)	60.83 (0.7)	51.48 (0.8)	51.60 (0.9)

Table 3: Comparison of OOD detection by AUROC (%) (\uparrow) between MOON +KNN, MOON +KLM and baseline post-process methods (i.e., KNN and KLM) for CIFAR-10 using RigL (80%, 90%, 95%, 99% sparsity). Our MOON leads to larger AUROC on each OOD data, showing its ability to improve reliability on OOD data in sparse training.

		CIFAR-100	TIN	NearOOD	MNIST	SVHN	Texture	Places365	FarOOD
80%	KNN	89.50	91.12	90.31	94.11	93.76	92.69	90.83	92.85
	<i>MOON +KNN</i>	90.16	92.11	91.14	95.58	93.77	94.02	92.47	93.96
	KLM	77.29	78.98	78.14	83.65	86.22	80.29	77.89	82.01
	<i>MOON +KLM</i>	78.92	81.92	80.42	89.29	86.44	84.78	80.23	85.18
90%	KNN	88.49	90.54	89.51	92.93	92.12	92.06	89.98	91.77
	<i>MOON +KNN</i>	89.40	91.32	90.36	95.04	93.97	92.99	91.73	93.43
	KLM	77.60	79.66	78.63	87.9	85.58	80.93	76.64	82.76
	<i>MOON +KLM</i>	79.21	81.29	80.25	89.38	89.94	83.33	80.04	85.67
95%	KNN	88.10	89.87	88.98	94.85	93.10	92.60	89.50	92.51
	<i>MOON +KNN</i>	88.36	90.34	89.35	94.98	93.62	92.91	90.51	93.01
	KLM	76.56	78.34	77.45	87.84	78.86	77.67	76.15	80.13
	<i>MOON +KLM</i>	79.06	81.26	80.16	89.64	84.04	83.59	79.35	84.16
99%	KNN	81.87	84.18	83.03	92.69	86.00	86.15	82.96	86.95
	<i>MOON +KNN</i>	82.97	84.78	83.88	96.62	95.64	89.15	83.03	91.11
	KLM	72.27	74.47	73.37	78.44	65.96	74.22	73.64	73.06
	<i>MOON +KLM</i>	75.40	76.63	76.01	85.03	82.32	78.51	74.90	80.19

represent the FPR-95 of MOON and calibration methods, respectively. We can see that the red hexagons are smaller than the blue hexagons, indicating better OOD detection from MOON compared to calibration methods.

5.3 ID Test Accuracy and Reliability in Sparse Training

In this section, we show that, in addition to improving OOD detection, our MOON can also maintain or improve the accuracy and reliability on ID data. We incorporate our MOON into sparse training (RigL) and compare it with the original sparse training results without MOON.

For ID Test Accuracy, as shown in Figure 4 (a)-(b), the red and blue curves represent our MOON +RigL and RigL, respectively. The red curve is usually higher or equal to the blue curve, implying that our MOON can maintain comparable or higher test accuracy on the ID data.

For ID Reliability, we choose expected calibration error (ECE) (Guo et al., 2017), a widely-used measure of the discrepancy between a model’s confidence and true accuracy, where a lower ECE indicates better confidence calibration and higher reliability. As shown in Figure 4 (c)-(d), the red and blue curves represent our MOON+RigL and RigL, respectively, where the colored arcs represent the 95% confidence intervals. The

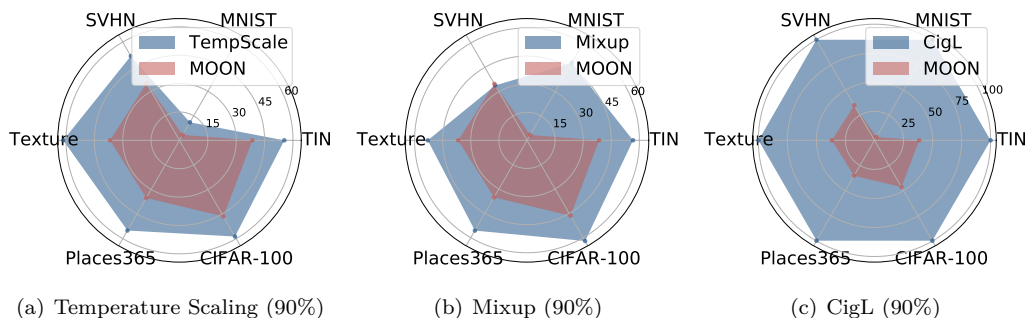


Figure 3: Comparison of OOD detection by FPR-95 (%) (\downarrow) on CIFAR-10 between MOON and other calibration methods using RigL (90%). The red hexagons (MOON) are smaller than the blue hexagons (other calibration methods), indicating a better OOD detection using MOON compared to (a) Temperature Scaling, (b) Mixup, and (c) CigL.

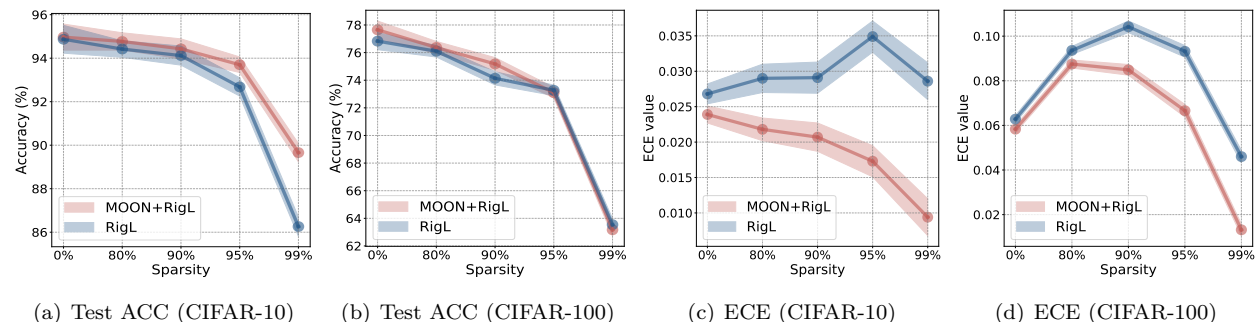


Figure 4: Comparison of performance on ID data by ECE (\downarrow) and test accuracy (ACC) (%) (\uparrow) between MOON and RigL. Our MOON leads to smaller ECE and maintains comparable or higher test accuracy on ID data, showing its ability to improve reliability on ID data.

red curve is usually lower than the blue curve. This shows that our MOON reduces the ECE, implying an improvement in the ID reliability of our MOON.

Table 4: Comparison of reliability of ID and OOD data between MOON +MSP (*M-MSP*) and MSP for CIFAR-10 in sparse training using SET. Our MOON leads to smaller ECE and comparable or higher accuracy (ACC) (%) on ID data, and smaller FPR-95 (%) on each OOD data compared to baseline method MSP, showing its ability to improve reliability on ID and OOD data.

	ID DATA		OOD DATA (FPR-95 (%) (\downarrow))					
	ECE(\downarrow)	ACC (\uparrow)	CIFAR-100	TIN	MNIST	SVHN	TEXTURE	PLACES365
80%	MSP	0.031 (0.002) 94.03 (0.2)	64.01 (0.5)	60.64 (0.4)	46.62 (1.2)	66.43 (1.4)	64.50 (0.7)	60.63 (0.4)
	<i>M-MSP</i>	0.020 (0.001) 94.80 (0.2)	62.72 (0.4)	58.63 (0.3)	47.63 (1.5)	60.68 (1.2)	59.10 (0.8)	59.39 (0.3)
90%	MSP	0.032 (0.001) 93.94 (0.2)	64.70 (0.3)	62.52 (0.4)	50.45 (1.6)	67.50 (1.7)	64.13 (0.6)	63.33 (0.4)
	<i>M-MSP</i>	0.019 (0.001) 94.44 (0.3)	63.33 (0.3)	60.15 (0.5)	43.02 (1.2)	58.81 (2.2)	61.26 (0.6)	60.79 (0.4)
95%	MSP	0.035 (0.002) 92.56 (0.3)	67.62 (0.5)	65.18 (0.4)	51.79 (1.7)	67.95 (1.5)	67.46 (0.7)	65.44 (0.5)
	<i>M-MSP</i>	0.020 (0.003) 93.59 (0.3)	63.69 (0.5)	60.20 (0.5)	41.82 (1.9)	62.02 (1.1)	57.29 (0.8)	60.85 (0.4)
99%	MSP	0.025 (0.001) 87.58 (0.2)	74.98 (0.4)	73.27 (0.5)	54.12 (1.5)	74.44 (1.2)	74.36 (0.7)	74.03 (0.3)
	<i>M-MSP</i>	0.008 (0.002) 88.67 (0.2)	71.88 (0.5)	69.59 (0.5)	45.14 (1.4)	71.10 (1.1)	65.73 (0.9)	71.61 (0.3)

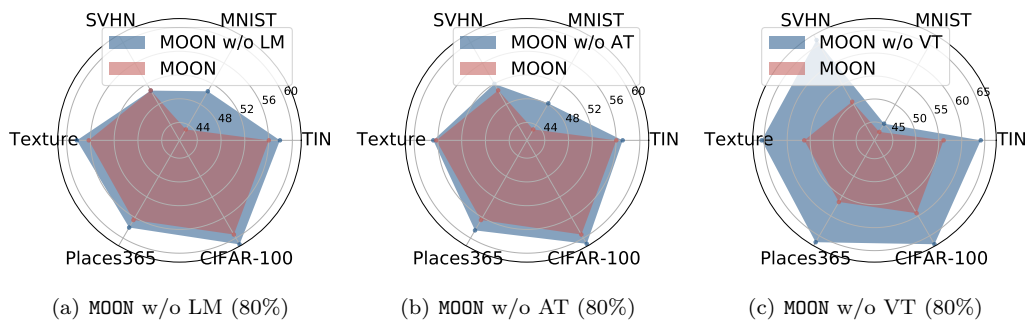


Figure 5: Ablation studies: comparison of FPR-95 (%) (\downarrow) between MOON, MOON w/o LM, MOON w/o AT, and MOON w/o VT on OOD data of CIFAR-10. MOON produces lower FPR-95 compared to the other three methods.

Table 5: Comparison of OOD detection by AUROC (%) (\uparrow) between MOON +MSP (*M-MSP*), LogitNorm+MSP (L-MSP), and VOS+MSP (V-MSP) for CIFAR-10 in sparse training. Our MOON leads to larger AUROC on each OOD data of CIFAR-10, showing its ability to improve OOD reliability.

		CIFAR-100	TIN	NEAROOD	MNIST	SVHN	TEXTURE	PLACES365	FAROOD
80%	L-MSP	87.71	89.60	88.66	94.74	93.29	89.36	90.79	92.05
	V-MSP	87.57	89.04	88.31	91.82	90.93	89.42	88.60	90.19
	M-MSP	89.93	91.14	90.53	95.00	93.82	91.80	90.82	92.86
90%	L-MSP	87.81	89.41	88.61	95.37	91.26	90.24	89.85	91.68
	V-MSP	87.48	88.58	88.03	92.97	92.17	88.93	88.81	90.53
	M-MSP	88.92	90.34	89.63	95.39	93.09	91.09	89.92	92.37
95%	L-MSP	87.35	88.58	87.96	93.36	86.36	87.79	88.49	89.03
	V-MSP	87.12	87.98	87.55	93.64	86.40	88.10	87.89	89.01
	M-MSP	88.04	89.39	88.71	94.76	93.35	89.86	88.51	91.62
99%	L-MSP	82.60	84.52	83.56	91.75	87.56	84.16	82.68	86.54
	V-MSP	82.22	83.09	82.65	84.75	89.99	82.75	82.26	84.69
	M-MSP	83.75	85.11	84.43	91.96	89.01	86.44	83.38	87.70

5.4 Comparison with Other Sparse Training Method

Apart from the comparison based on RigL, we also include sparse training results using SET (Mocanu et al., 2018) on CIFAR-10 at 80%, 90%, 95%, 99% sparsities. As shown in Table 4, on OOD data, our MOON also leads to smaller FPR-95, indicating improved OOD reliability from our MOON. On ID data, our MOON brings smaller ECE and comparable or higher accuracy (ACC), implying comparable or improved ID reliability and performance. This shows our MOON is effective in different sparse training methods.

5.5 Comparison with Other Training-time Regularization Method

Since our loss modification can be viewed as a new type of training-time regularization, we also add additional experiments on other dense training-time regularization methods including LogitNorm (Wei et al., 2022a) and VOS (Du et al., 2022). As shown in Table 5, our method MOON has larger AUROC compared to LogitNorm and VOS, indicating better OOD reliability from our method in sparse training.

5.6 Comparison with Other Extra-dimension Method

Since our loss modification also belongs to the extra-dimension method, we further compare our MOON with another extra-dimension method, i.e., DAC (Thulasidasan et al., 2019) regarding the reliability of ID and OOD data. As shown in Table 6, our MOON also provides larger AUROC when given OOD data. When faced with ID data, our MOON leads to smaller ECE and comparable or higher accuracy (ACC). This suggests that

Table 6: Comparison of reliability of ID and OOD data between MOON and DAC for CIFAR-10 and CIFAR-100. Our MOON leads to smaller ECE and comparable or higher accuracy (ACC) on ID data, and larger AUROC on each OOD data, showing its ability to improve reliability on ID and OOD data.

DATA	METHOD	ID DATA		OOD DATA (AUROC (\uparrow))					
		ECE(\downarrow)	ACC(\uparrow)	CIFAR-100/10	TIN	MNIST	SVHN	TEXTURE	PLACES365
CIFAR-10	DAC	0.0302	94.43	86.17	87.96	89.92	87.26	89.32	88.48
	MOON	0.0239	94.97	89.93	91.14	95.00	93.82	91.80	90.82
CIFAR-100	DAC	0.0873	76.03	76.99	80.54	74.43	77.70	77.89	77.86
	MOON	0.0583	77.65	78.82	82.38	80.28	81.57	77.62	79.65

Table 7: Ablation studies: comparison of ECE (\downarrow) and accuracy (ACC, \uparrow) between MOON, MOON w/o LM, MOON w/o AT, and MOON w/o VT on CIFAR-100. MOON produces lower ECE values and comparable or higher accuracy.

METHOD	80%		90%		95%		99%	
	ECE (\downarrow)	ACC (%) (\uparrow)	ECE (\downarrow)	ACC (%) (\uparrow)	ECE (\downarrow)	ACC (%) (\uparrow)	ECE (\downarrow)	ACC (%) (\uparrow)
MOON w/o LM	0.0272	94.68	0.0282	94.40	0.0307	93.44	0.0207	89.63
MOON w/o AT	0.0250	94.81	0.0258	94.51	0.0308	93.26	0.0200	89.50
MOON w/o VT	0.0296	92.97	0.0256	91.81	0.0330	90.23	0.0096	85.38
MOON	0.0218	94.77	0.0207	94.53	0.0173	93.70	0.0094	89.66

our MOON makes better use of the additional dimension to encourage the model to think about the unknown, thus improving real-world reliability while maintaining ID performance and reliability.

5.7 Ablation Studies

We do ablation studies to demonstrate the importance of each component in our MOON, where we train CIFAR-100 using our MOON without the unknown-aware loss modification (MOON w/o LM), MOON without the auto-tuning strategy (MOON w/o AT), and MOON without the average-based voting scheme (MOON w/o VT), respectively. The OOD detection is shown by FPR-95 for each OOD data of CIFAR-100 in Figure 5, and the ID results are summarized in Table 7.

MOON w/o LM: As shown in Figure 5 (a), the blue hexagon (MOON w/o LM) is larger than the red hexagon (MOON), indicating a decrease in OOD reliability without the unknown-aware loss modification. Table 7 also shows an increased ECE and decreased ID reliability in MOON w/o LM.

MOON w/o AT: Similarly, as depicted in Figure 5 (b), the blue hexagon (MOON w/o AT) is larger than the red hexagon (MOON), indicating a decrease in OOD reliability in the absence of the auto-tuning strategy. Table 7 also shows an increased ECE and decreased ID reliability in MOON w/o AT.

MOON w/o VT: As summarized in Figure 5 (c), the blue hexagon (MOON w/o VT) is larger than the red hexagon (MOON), indicating a decrease in OOD reliability when no average-based voting scheme is present. Table 7 further shows a decreased accuracy and increased ECE in MOON w/o VT.

6 Conclusion and Limitations

We investigate for the first time the reliability of sparse training from an OOD perspective, which jointly considers OOD reliability and efficiency and has important implications for real-world DNN applications. We observe that sparse training causes more severe unreliability, with useful unknown information being ignored in the training. Thus, we propose a new unknown-aware sparse training method, MOON, to enhance OOD detection under sparsity constraints, with little additional cost and no extra OOD data requirement.

We provide theoretical insights to demonstrate the lower confidence brought by MOON on OOD samples. We also conduct extensive experiments on multiple benchmark datasets, architectures, and sparsities, showing that our MOON can improve AUROC by up to 8.4%. Our MOON can be used as a drop-in replacement for existing sparse training methods, which fills an important gap in sparse training and improves the effectiveness and applicability of the sparse training paradigm.

Despite the enhanced OOD reliability achieved in sparse training, MOON does not address this matter comprehensively from a broader reliability perspective, including robust generalization (Silva & Najafirad, 2020; Özdenizci & Legenstein, 2021; Chen et al., 2022a) and adaptation (Emam et al., 2021; Alayrac et al., 2022; Hu et al., 2022), which are equally vital aspects of reliability and deserve further investigation (Tran et al., 2022). Additionally, the effectiveness of MOON remains unexplored in the context of widely employed large generative models (Ouyang et al., 2022; Xu et al., 2023; Croitoru et al., 2023). On the one hand, as model size expands, novel changes in model characteristics may arise (Wei et al., 2022b). On the other hand, given the prevalence of non-classification tasks within LLMs, the exploration of how to evaluate their reliability remains an uncharted domain.

References

- Faruk Ahmed and Aaron Courville. Detecting semantic anomalies. In *Proceedings of the AAAI Conference on Artificial Intelligence*, volume 34, pp. 3154–3162, 2020.
- Nilesh A Ahuja, Ibrahima Ndiour, Trushant Kalyanpur, and Omesh Tickoo. Probabilistic modeling of deep features for out-of-distribution and adversarial detection. *arXiv preprint arXiv:1909.11786*, 2019.
- Jean-Baptiste Alayrac, Jeff Donahue, Pauline Luc, Antoine Miech, Iain Barr, Yana Hasson, Karel Lenc, Arthur Mensch, Katherine Millican, Malcolm Reynolds, et al. Flamingo: a visual language model for few-shot learning. *Advances in Neural Information Processing Systems*, 35:23716–23736, 2022.
- Arsenii Ashukha, Alexander Lyzhov, Dmitry Molchanov, and Dmitry Vetrov. Pitfalls of in-domain uncertainty estimation and ensembling in deep learning. *arXiv preprint arXiv:2002.06470*, 2020.
- Morgane Ayle, Bertrand Charpentier, John Rachwan, Daniel Zügner, Simon Geisler, and Stephan Günnemann. On the robustness and anomaly detection of sparse neural networks. *arXiv preprint arXiv:2207.04227*, 2022.
- Guillaume Bellec, David Kappel, Wolfgang Maass, and Robert Legenstein. Deep rewiring: Training very sparse deep networks. *arXiv preprint arXiv:1711.05136*, 2017.
- Guillaume Bellec, David Kappel, Wolfgang Maass, and Robert Legenstein. Deep rewiring: Training very sparse deep networks. *International Conference on Learning Representations (ICLR)*, 2018.
- Abhijit Bendale and Terrance E Boult. Towards open set deep networks. In *Proceedings of the IEEE conference on computer vision and pattern recognition*, pp. 1563–1572, 2016.
- Sameer Bibikar, Haris Vikalo, Zhangyang Wang, and Xiaohan Chen. Federated dynamic sparse training: Computing less, communicating less, yet learning better. In *Proceedings of the AAAI Conference on Artificial Intelligence*, volume 36, pp. 6080–6088, 2022.
- Varun Chandola, Arindam Banerjee, and Vipin Kumar. Anomaly detection: A survey. *ACM computing surveys (CSUR)*, 41(3):1–58, 2009.
- Tianlong Chen, Zhenyu Zhang, Pengjun Wang, Santosh Balachandra, Haoyu Ma, Zehao Wang, and Zhangyang Wang. Sparsity winning twice: Better robust generalization from more efficient training. *arXiv preprint arXiv:2202.09844*, 2022a.
- Tianlong Chen, Zhenyu Zhang, Jun Wu, Randy Huang, Sijia Liu, Shiyu Chang, and Zhangyang Wang. Can you win everything with a lottery ticket? *Transactions on Machine Learning Research*, 2022b.

- Zhen Cheng, Fei Zhu, Xu-Yao Zhang, and Cheng-Lin Liu. Average of pruning: Improving performance and stability of out-of-distribution detection. *arXiv preprint arXiv:2303.01201*, 2023.
- Florinel-Alin Croitoru, Vlad Hondru, Radu Tudor Ionescu, and Mubarak Shah. Diffusion models in vision: A survey. *IEEE Transactions on Pattern Analysis and Machine Intelligence*, 2023.
- Lavindra De Silva and Alan Mycroft. Toward trustworthy programming for autonomous concurrent systems. *AI & SOCIETY*, pp. 1–3, 2022.
- Li Deng. The mnist database of handwritten digit images for machine learning research [best of the web]. *IEEE signal processing magazine*, 29(6):141–142, 2012.
- Tim Dettmers and Luke Zettlemoyer. Sparse networks from scratch: Faster training without losing performance. *arXiv preprint arXiv:1907.04840*, 2019.
- Terrance DeVries and Graham W Taylor. Learning confidence for out-of-distribution detection in neural networks. *arXiv preprint arXiv:1802.04865*, 2018.
- Xuefeng Du, Zhaoning Wang, Mu Cai, and Yixuan Li. Vos: Learning what you don’t know by virtual outlier synthesis. *arXiv preprint arXiv:2202.01197*, 2022.
- Zeyad Ali Sami Emam, Hong-Min Chu, Ping-Yeh Chiang, Wojciech Czaja, Richard Leapman, Micah Goldblum, and Tom Goldstein. Active learning at the imagenet scale. *arXiv preprint arXiv:2111.12880*, 2021.
- Utku Evci, Fabian Pedregosa, Aidan Gomez, and Erich Elsen. The difficulty of training sparse neural networks. *arXiv preprint arXiv:1906.10732*, 2019.
- Utku Evci, Trevor Gale, Jacob Menick, Pablo Samuel Castro, and Erich Elsen. Rigging the lottery: Making all tickets winners. In *International Conference on Machine Learning*, pp. 2943–2952. PMLR, 2020.
- Yarin Gal and Zoubin Ghahramani. Dropout as a bayesian approximation: Representing model uncertainty in deep learning. In *international conference on machine learning*, pp. 1050–1059. PMLR, 2016.
- Chuan Guo, Geoff Pleiss, Yu Sun, and Kilian Q Weinberger. On calibration of modern neural networks. In *International conference on machine learning*, pp. 1321–1330. PMLR, 2017.
- Songqiao Han, Xiyang Hu, Hailiang Huang, Mingqi Jiang, and Yue Zhao. Adbench: Anomaly detection benchmark. *arXiv preprint arXiv:2206.09426*, 2022.
- Kaiming He, Xiangyu Zhang, Shaoqing Ren, and Jian Sun. Deep residual learning for image recognition. In *Proceedings of the IEEE conference on computer vision and pattern recognition*, pp. 770–778, 2016.
- Zheng He, Zeke Xie, Quanzhi Zhu, and Zengchang Qin. Sparse double descent: Where network pruning aggravates overfitting. In *International Conference on Machine Learning*, pp. 8635–8659. PMLR, 2022.
- Dan Hendrycks and Kevin Gimpel. A baseline for detecting misclassified and out-of-distribution examples in neural networks. *arXiv preprint arXiv:1610.02136*, 2016.
- Dan Hendrycks, Mantas Mazeika, and Thomas Dietterich. Deep anomaly detection with outlier exposure. *arXiv preprint arXiv:1812.04606*, 2018.
- Dan Hendrycks, Steven Basart, Mantas Mazeika, Andy Zou, Joe Kwon, Mohammadreza Mostajabi, Jacob Steinhardt, and Dawn Song. Scaling out-of-distribution detection for real-world settings. In *International Conference on Machine Learning*, pp. 8759–8773. PMLR, 2022.
- Yen-Chang Hsu, Yilin Shen, Hongxia Jin, and Zsolt Kira. Generalized odin: Detecting out-of-distribution image without learning from out-of-distribution data. In *Proceedings of the IEEE/CVF Conference on Computer Vision and Pattern Recognition*, pp. 10951–10960, 2020.

- Shell Xu Hu, Da Li, Jan Stühmer, Minyoung Kim, and Timothy M Hospedales. Pushing the limits of simple pipelines for few-shot learning: External data and fine-tuning make a difference. In *Proceedings of the IEEE/CVF Conference on Computer Vision and Pattern Recognition*, pp. 9068–9077, 2022.
- Shaoyi Huang, Bowen Lei, Dongkuan Xu, Hongwu Peng, Yue Sun, Mimi Xie, and Caiwen Ding. Dynamic sparse training via balancing the exploration-exploitation trade-off. *arXiv preprint arXiv:2211.16667*, 2022.
- Shaoyi Huang, Haowen Fang, Kaleel Mahmood, Bowen Lei, Nuo Xu, Bin Lei, Yue Sun, Dongkuan Xu, Wujie Wen, and Caiwen Ding. Neurogenesis dynamics-inspired spiking neural network training acceleration. *arXiv preprint arXiv:2304.12214*, 2023.
- Pavel Izmailov, Dmitrii Podoprikin, Timur Garipov, Dmitry Vetrov, and Andrew Gordon Wilson. Averaging weights leads to wider optima and better generalization. *arXiv preprint arXiv:1803.05407*, 2018.
- Siddhant Jayakumar, Razvan Pascanu, Jack Rae, Simon Osindero, and Erich Elsen. Top-kast: Top-k always sparse training. *Advances in Neural Information Processing Systems*, 33:20744–20754, 2020.
- Alex Krizhevsky, Geoffrey Hinton, et al. Learning multiple layers of features from tiny images. *Technical report, University of Toronto*, 2009.
- Kimin Lee, Kibok Lee, Honglak Lee, and Jinwoo Shin. A simple unified framework for detecting out-of-distribution samples and adversarial attacks. *Advances in neural information processing systems*, 31, 2018.
- Bowen Lei, Dongkuan Xu, Ruqi Zhang, Shuren He, and Bani K Mallick. Balance is essence: Accelerating sparse training via adaptive gradient correction. *arXiv preprint arXiv:2301.03573*, 2023a.
- Bowen Lei, Ruqi Zhang, Dongkuan Xu, and Bani Mallick. Calibrating the rigged lottery: Making all tickets reliable. *International Conference on Learning Representations (ICLR)*, 2023b.
- Chun-Liang Li, Kihyuk Sohn, Jinsung Yoon, and Tomas Pfister. Cutpaste: Self-supervised learning for anomaly detection and localization. In *Proceedings of the IEEE/CVF Conference on Computer Vision and Pattern Recognition*, pp. 9664–9674, 2021.
- Shiyu Liang, Yixuan Li, and Rayadurgam Srikant. Enhancing the reliability of out-of-distribution image detection in neural networks. *arXiv preprint arXiv:1706.02690*, 2017.
- Chuang Liu, Xueqi Ma, Yinbing Zhan, Liang Ding, Dapeng Tao, Bo Du, Wenbin Hu, and Danilo Mandic. Comprehensive graph gradual pruning for sparse training in graph neural networks. *arXiv preprint arXiv:2207.08629*, 2022a.
- Shiwei Liu, Tianlong Chen, Zahra Atashgahi, Xiaohan Chen, Ghada Sokar, Elena Mocanu, Mykola Pechenizkiy, Zhangyang Wang, and Decebal Constantin Mocanu. Deep ensembling with no overhead for either training or testing: The all-round blessings of dynamic sparsity. *arXiv preprint arXiv:2106.14568*, 2021a.
- Shiwei Liu, Lu Yin, Decebal Constantin Mocanu, and Mykola Pechenizkiy. Do we actually need dense over-parameterization? in-time over-parameterization in sparse training. In *International Conference on Machine Learning*, pp. 6989–7000. PMLR, 2021b.
- Shiwei Liu, Tianlong Chen, Xiaohan Chen, Li Shen, Decebal Constantin Mocanu, Zhangyang Wang, and Mykola Pechenizkiy. The unreasonable effectiveness of random pruning: Return of the most naive baseline for sparse training. *arXiv preprint arXiv:2202.02643*, 2022b.
- Weitang Liu, Xiaoyun Wang, John Owens, and Yixuan Li. Energy-based out-of-distribution detection. *Advances in Neural Information Processing Systems*, 33:21464–21475, 2020.
- Yixin Liu, Kaize Ding, Huan Liu, and Shirui Pan. Good-d: On unsupervised graph out-of-distribution detection. In *Proceedings of the Sixteenth ACM International Conference on Web Search and Data Mining*, pp. 339–347, 2023.

- Decebal Constantin Mocanu, Elena Mocanu, Peter Stone, Phuong H Nguyen, Madeleine Gibescu, and Antonio Liotta. Scalable training of artificial neural networks with adaptive sparse connectivity inspired by network science. *Nature communications*, 9(1):1–12, 2018.
- Peyman Morteza and Yixuan Li. Provable guarantees for understanding out-of-distribution detection. In *Proceedings of the AAAI Conference on Artificial Intelligence*, volume 36, pp. 7831–7840, 2022.
- Hesham Mostafa and Xin Wang. Parameter efficient training of deep convolutional neural networks by dynamic sparse reparameterization. In *International Conference on Machine Learning*, pp. 4646–4655. PMLR, 2019.
- Hussein Mozannar and David Sontag. Consistent estimators for learning to defer to an expert. In *International Conference on Machine Learning*, pp. 7076–7087. PMLR, 2020.
- Yuval Netzer, Tao Wang, Adam Coates, Alessandro Bissacco, Bo Wu, and Andrew Y Ng. Reading digits in natural images with unsupervised feature learning. 2011.
- Jeremy Nixon, Michael W Dusenberry, Linchuan Zhang, Ghassen Jerfel, and Dustin Tran. Measuring calibration in deep learning. In *CVPR Workshops*, volume 2, 2019.
- Long Ouyang, Jeffrey Wu, Xu Jiang, Diogo Almeida, Carroll Wainwright, Pamela Mishkin, Chong Zhang, Sandhini Agarwal, Katarina Slama, Alex Ray, et al. Training language models to follow instructions with human feedback. *Advances in Neural Information Processing Systems*, 35:27730–27744, 2022.
- Ozan Özdenizci and Robert Legenstein. Training adversarially robust sparse networks via bayesian connectivity sampling. In *International Conference on Machine Learning*, pp. 8314–8324. PMLR, 2021.
- Shreyas Padhy, Zachary Nado, Jie Ren, Jeremiah Liu, Jasper Snoek, and Balaji Lakshminarayanan. Revisiting one-vs-all classifiers for predictive uncertainty and out-of-distribution detection in neural networks. *arXiv preprint arXiv:2007.05134*, 2020.
- Kanil Patel, William Beluch, Kilian Rambach, Michael Pfeiffer, and Bin Yang. Improving uncertainty of deep learning-based object classification on radar spectra using label smoothing. In *2022 IEEE Radar Conference (RadarConf22)*, pp. 1–6. IEEE, 2022.
- Rahul Rahaman et al. Uncertainty quantification and deep ensembles. *Advances in Neural Information Processing Systems*, 34:20063–20075, 2021.
- Khansa Rasheed, Adnan Qayyum, Mohammed Ghaly, Ala Al-Fuqaha, Adeel Razi, and Junaid Qadir. Explainable, trustworthy, and ethical machine learning for healthcare: A survey. *Computers in Biology and Medicine*, pp. 106043, 2022.
- Abhijit Guha Roy, Jie Ren, Shekoofeh Azizi, Aaron Loh, Vivek Natarajan, Basil Mustafa, Nick Pawlowski, Jan Freyberg, Yuan Liu, Zach Beaver, et al. Does your dermatology classifier know what it doesn’t know? detecting the long-tail of unseen conditions. *Medical Image Analysis*, 75:102274, 2022.
- Olga Russakovsky, Jia Deng, Hao Su, Jonathan Krause, Sanjeev Satheesh, Sean Ma, Zhiheng Huang, Andrej Karpathy, Aditya Khosla, Michael Bernstein, et al. Imagenet large scale visual recognition challenge. *International journal of computer vision*, 115(3):211–252, 2015.
- Jonathan Schwarz, Siddhant Jayakumar, Razvan Pascanu, Peter E Latham, and Yee Teh. Powerpropagation: A sparsity inducing weight reparameterisation. *Advances in Neural Information Processing Systems*, 34:28889–28903, 2021.
- Connor Shorten and Taghi M Khoshgoftaar. A survey on image data augmentation for deep learning. *Journal of big data*, 6(1):1–48, 2019.
- Samuel Henrique Silva and Peyman Najafirad. Opportunities and challenges in deep learning adversarial robustness: A survey. *arXiv preprint arXiv:2007.00753*, 2020.

- Ghada Sokar, Elena Mocanu, Decebal Constantin Mocanu, Mykola Pechenizkiy, and Peter Stone. Dynamic sparse training for deep reinforcement learning. *arXiv preprint arXiv:2106.04217*, 2021.
- Yiyu Sun and Yixuan Li. On the effectiveness of sparsification for detecting the deep unknowns. *arXiv preprint arXiv:2111.09805*, 2021.
- Yiyu Sun, Yifei Ming, Xiaojin Zhu, and Yixuan Li. Out-of-distribution detection with deep nearest neighbors. *arXiv preprint arXiv:2204.06507*, 2022.
- Varun Sundar and Rajat Vadiraj Dwaraknath. [reproducibility report] rigging the lottery: Making all tickets winners. *arXiv preprint arXiv:2103.15767*, 2021.
- Christian Szegedy, Vincent Vanhoucke, Sergey Ioffe, Jon Shlens, and Zbigniew Wojna. Rethinking the inception architecture for computer vision. In *Proceedings of the IEEE conference on computer vision and pattern recognition*, pp. 2818–2826, 2016.
- David Martinus Johannes Tax. One-class classification: Concept learning in the absence of counter-examples. 2002.
- Sunil Thulasidasan, Tanmoy Bhattacharya, Jeff Bilmes, Gopinath Chennupati, and Jamal Mohd-Yusof. Combating label noise in deep learning using abstention. *arXiv preprint arXiv:1905.10964*, 2019.
- Antonio Torralba, Rob Fergus, and William T Freeman. 80 million tiny images: A large data set for nonparametric object and scene recognition. *IEEE transactions on pattern analysis and machine intelligence*, 30(11):1958–1970, 2008.
- Dustin Tran, Jeremiah Liu, Michael W Dusenberry, Du Phan, Mark Collier, Jie Ren, Kehang Han, Zi Wang, Zeldia Mariet, Huiyi Hu, et al. Plex: Towards reliability using pretrained large model extensions. *arXiv preprint arXiv:2207.07411*, 2022.
- Sagar Vaze, Kai Han, Andrea Vedaldi, and Andrew Zisserman. Open-set recognition: A good closed-set classifier is all you need. *arXiv preprint arXiv:2110.06207*, 2021.
- Rajeev Verma and Eric Nalisnick. Calibrated learning to defer with one-vs-all classifiers. In *International Conference on Machine Learning*, pp. 22184–22202. PMLR, 2022.
- Deng-Bao Wang, Lei Feng, and Min-Ling Zhang. Rethinking calibration of deep neural networks: Do not be afraid of overconfidence. *Advances in Neural Information Processing Systems*, 34:11809–11820, 2021a.
- Yezhen Wang, Bo Li, Tong Che, Kaiyang Zhou, Ziwei Liu, and Dongsheng Li. Energy-based open-world uncertainty modeling for confidence calibration. In *Proceedings of the IEEE/CVF International Conference on Computer Vision*, pp. 9302–9311, 2021b.
- Hongxin Wei, Renchunzi Xie, Hao Cheng, Lei Feng, Bo An, and Yixuan Li. Mitigating neural network overconfidence with logit normalization. In *International Conference on Machine Learning*, pp. 23631–23644. PMLR, 2022a.
- Jason Wei, Yi Tay, Rishi Bommasani, Colin Raffel, Barret Zoph, Sebastian Borgeaud, Dani Yogatama, Maarten Bosma, Denny Zhou, Donald Metzler, et al. Emergent abilities of large language models. *arXiv preprint arXiv:2206.07682*, 2022b.
- Mitchell Wortsman, Gabriel Ilharco, Samir Ya Gadre, Rebecca Roelofs, Raphael Gontijo-Lopes, Ari S Morcos, Hongseok Namkoong, Ali Farhadi, Yair Carmon, Simon Kornblith, et al. Model soups: averaging weights of multiple fine-tuned models improves accuracy without increasing inference time. In *International Conference on Machine Learning*, pp. 23965–23998. PMLR, 2022.
- Longfeng Wu, Bowen Lei, Dongkuan Xu, and Dawei Zhou. Towards reliable rare category analysis on graphs via individual calibration. In *Proceedings of the 29th ACM SIGKDD Conference on Knowledge Discovery and Data Mining*, pp. 2629–2638, 2023.

- Binfeng Xu, Zhiyuan Peng, Bowen Lei, Subhabrata Mukherjee, Yuchen Liu, and Dongkuan Xu. Rewoo: Decoupling reasoning from observations for efficient augmented language models. *arXiv preprint arXiv:2305.18323*, 2023.
- Jingkang Yang, Haoqi Wang, Litong Feng, Xiaopeng Yan, Huabin Zheng, Wayne Zhang, and Ziwei Liu. Semantically coherent out-of-distribution detection. In *Proceedings of the IEEE/CVF International Conference on Computer Vision*, pp. 8301–8309, 2021a.
- Jingkang Yang, Kaiyang Zhou, Yixuan Li, and Ziwei Liu. Generalized out-of-distribution detection: A survey. *arXiv preprint arXiv:2110.11334*, 2021b.
- Jingkang Yang, Pengyun Wang, Dejian Zou, Zitang Zhou, Kunyuan Ding, Wenxuan Peng, Haoqi Wang, Guangyao Chen, Bo Li, Yiyu Sun, et al. Openood: Benchmarking generalized out-of-distribution detection. *arXiv preprint arXiv:2210.07242*, 2022.
- Lu Yin, Vlado Menkovski, Meng Fang, Tianjin Huang, Yulong Pei, Mykola Pechenizkiy, Decebal Constantin Mocanu, and Shiwei Liu. Superposing many tickets into one: A performance booster for sparse neural network training. *arXiv preprint arXiv:2205.15322*, 2022.
- Qing Yu and Kiyoharu Aizawa. Unsupervised out-of-distribution detection by maximum classifier discrepancy. In *Proceedings of the IEEE/CVF international conference on computer vision*, pp. 9518–9526, 2019.
- Geng Yuan, Xiaolong Ma, Wei Niu, Zhengang Li, Zhenglun Kong, Ning Liu, Yifan Gong, Zheng Zhan, Chaoyang He, Qing Jin, et al. Mest: Accurate and fast memory-economic sparse training framework on the edge. *Advances in Neural Information Processing Systems*, 34:20838–20850, 2021.
- Hongyi Zhang, Moustapha Cisse, Yann N Dauphin, and David Lopez-Paz. mixup: Beyond empirical risk minimization. *arXiv preprint arXiv:1710.09412*, 2017.
- Jize Zhang, Bhavya Kaikhura, and T Yong-Jin Han. Mix-n-match: Ensemble and compositional methods for uncertainty calibration in deep learning. In *International conference on machine learning*, pp. 11117–11128. PMLR, 2020.
- Xiao Zhou, Weizhong Zhang, Hang Xu, and Tong Zhang. Effective sparsification of neural networks with global sparsity constraint. In *Proceedings of the IEEE/CVF Conference on Computer Vision and Pattern Recognition*, pp. 3599–3608, 2021.
- Dongyao Zhu, Bowen Lei, Jie Zhang, Yanbo Fang, Yiqun Xie, Ruqi Zhang, and Dongkuan Xu. Rethinking data distillation: Do not overlook calibration. In *Proceedings of the IEEE/CVF International Conference on Computer Vision*, pp. 4935–4945, 2023.

A Appendix: Additional Experimental Results

A.1 More Sparse Training Results

To further demonstrate the effectiveness of our MOON , apart from the comparison of AUROC (\uparrow) on CIFAR-10 in the main manuscript, we also include more comparison of FPR-95 (\downarrow) between MOON+MSP and MSP for CIFAR-10 in sparse training using RigL. As shown in Table 8, our MOON usually leads to smaller FPR-95, indicating more effective OOD detection from our MOON compared to baseline methods.

Table 8: Comparison of OOD detection by FPR-95 (\downarrow) between MOON+MSP and MSP for CIFAR-10 in sparse training using RigL. Our MOON leads to larger AUROC on each OOD data of CIFAR-10, showing its ability to improve reliability on OOD data.

		CIFAR-100	TIN	NEAROOD	MNIST	SVHN	TEXTURE	PLACES365	FAROOD
80%	MSP	62.97	59.71	61.34	48.16	53.70	60.35	58.59	55.20
	MOON+MSP	59.31	56.04	57.68	39.12	50.71	56.28	56.49	50.65
90%	MSP	63.71	61.54	62.62	54.85	58.33	66.76	61.43	60.34
	MOON+MSP	62.70	58.18	60.44	33.67	54.65	57.32	58.41	51.01
95%	MSP	70.38	66.96	68.67	44.19	74.57	73.01	65.37	64.28
	MOON+MSP	65.29	61.11	63.20	39.26	52.72	63.44	63.38	54.70
99%	MSP	77.34	73.71	75.53	60.45	77.77	71.54	76.49	71.56
	MOON+MSP	70.38	67.05	68.72	44.34	72.08	62.75	68.54	61.93

To show that the improvement from our MOON is consistent across different sparse training methods, apart from the comparison based on RigL, we also include more sparse training results using SET (Mocanu et al., 2018). As shown in Tables 9, our MOON usually leads to larger AUROC, indicating more effective OOD detection from our MOON compared to baseline methods.

Table 9: Comparison of OOD detection by AUROC (\uparrow) between MOON+MSP and MSP for CIFAR-10 in sparse training using SET. Our MOON leads to larger AUROC on each OOD data of CIFAR-10, showing its ability to improve reliability on OOD data.

		CIFAR-100	TIN	NEAROOD	MNIST	SVHN	TEXTURE	PLACES365	FAROOD
80%	MSP	87.36	88.81	88.09	93.41	88.70	88.51	88.77	89.85
	MOON+MSP	89.52	90.81	90.16	93.64	92.47	91.25	90.46	91.96
90%	MSP	87.93	89.06	88.49	93.54	90.26	88.40	88.57	90.19
	MOON+MSP	88.85	90.06	89.45	94.29	92.34	90.70	89.61	91.74
95%	MSP	86.81	87.83	87.32	94.95	89.13	87.07	87.62	89.69
	MOON+MSP	88.02	89.33	88.68	93.78	91.96	90.09	88.56	91.10
99%	MSP	81.79	82.41	82.10	90.13	87.08	81.31	81.77	85.07
	MOON+MSP	83.10	83.84	83.47	91.13	89.14	84.92	81.90	86.77

Prior work shows that calibration methods can help with OOD detection in dense DNNs (Wang et al., 2021b; Yang et al., 2022). To show the ineffectiveness of existing calibration methods for OOD detection in sparse training, we also compare our MOON to other confidence calibration methods including temperature scaling (Lee et al., 2018), Mixup (Zhang et al., 2017), and CigL (Lei et al., 2023b) using RigL for OOD detection capability in 99% sparsity. As shown in Figure 6, the red and blue hexagons represent the FPR-95 of MOON and other calibration methods, respectively. We can see that the red hexagons are smaller than the blue hexagons, indicating better OOD detection from MOON compared to other calibration methods.

To check the effectiveness of our MOON at low sparsity level, we add additional experiments at 50%, 60%, and 70% sparsity on CIFAR-10 and CIFAR-100. The detailed results are summarized in Figure 7. Our MOON can consistently improve the OOD reliability at different sparsity levels.

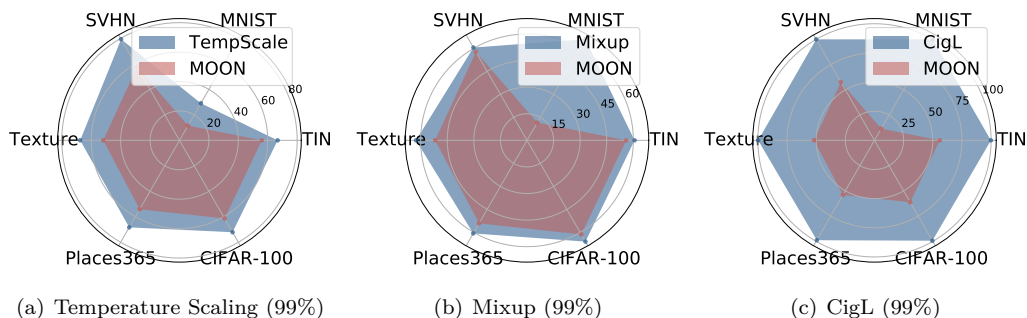


Figure 6: Comparison of OOD detection by FPR-95 (\downarrow) on CIFAR-10 between MOON and other calibration methods using RigL (90%). The red hexagons (MOON) are smaller than the blue hexagons (other calibration methods), indicating a better OOD detection using MOON compared to (a) Temperature Scaling, (b) Mixup, and (c) CigL.

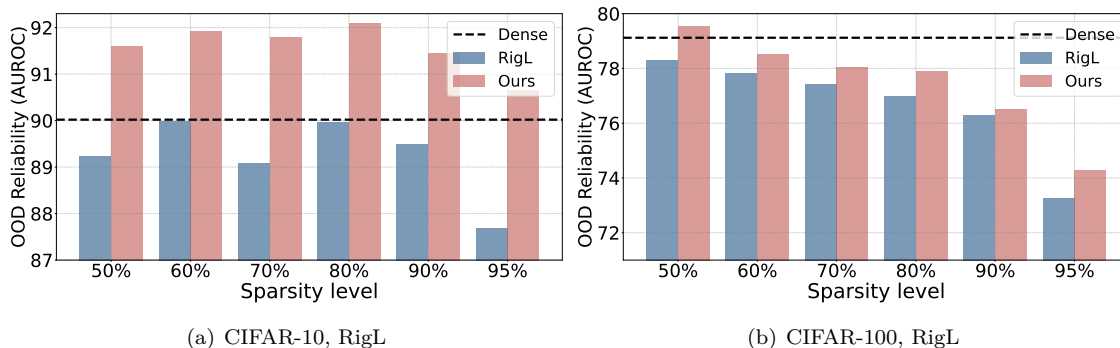


Figure 7: OOD reliability (measured by AUROC (%), the higher the better) of the ResNet-18 produced by dense and sparse training (RigL & SET) on CIFAR-10/100. Compared to dense training (black line), sparse training (blue bar) has a smaller AUROC, indicating sparse training exacerbates the unreliability on OOD data. Our MOON (red bar) improves AUROC and OOD detection.

Table 10: Comparison of OOD detection by FPR-95 (FPR, \downarrow) & AUROC (AUC, \uparrow) between MOON and MSP for MNIST. Our MOON leads to smaller FPR-95 and larger AUROC on each OOD data, showing its ability to improve reliability on OOD data.

		NOTMNIST	FASHIONMNIST	NEAROOD	TEXTURE	CIFAR10	TIN	PLACES365	FAROOD
FPR	MSP	40.81	30.46	35.64	7.43	7.11	6.11	9.28	7.48
	MOON+MSP	3.57	7.08	5.32	1.76	0.91	1.41	1.32	1.35
AUC	MSP	89.20	93.69	91.45	98.55	98.55	98.75	98.20	98.51
	MOON+MSP	98.07	96.54	97.31	98.86	99.18	99.06	99.12	99.05

A.2 More Results on MNIST

To show that the improvement from our MOON is consistent across different benchmark datasets, apart from the comparison on CIFAR-10, CIFAR-100, and ImageNet-2012, we also include more results on MNIST. As shown in Tables 10, our MOON usually leads to larger AUROC and smaller FPR-95, indicating more effective OOD detection from our MOON compared to baseline methods.

Table 11: Comparison of OOD detection by FPR-95 (\downarrow) & AUROC (\uparrow) between MOON and baseline post process methods for CIFAR-10. Our MOON leads to smaller FPR-95 and larger AUROC on each OOD data, showing its ability to improve reliability on OOD data.

		CIFAR-100	TIN	NEAROOD	MNIST	SVHN	TEXTURE	PLACES365	FAROOD
FPR-95	MSP	62.01	60.69	61.35	58.59	51.87	59.89	57.64	57.00
	MOON+MSP	61.01	56.87	58.94	40.91	48.25	51.31	57.56	49.50
	ODIN	59.09	59.06	59.07	36.23	67.92	51.10	50.51	51.44
	MOON+ODIN	48.47	42.24	45.36	8.10	33.30	32.58	40.64	28.65
	EBO	51.46	45.02	48.24	44.50	44.94	48.32	41.88	44.91
	MOON+EBO	47.41	39.29	43.35	14.98	21.34	36.75	38.51	27.90
AUROC	MSP	87.11	86.62	86.87	89.91	90.88	88.72	89.03	89.64
	MOON+MSP	89.06	90.61	89.83	94.11	93.83	92.30	89.97	92.55
	ODIN	77.68	77.33	77.51	90.91	73.32	80.70	82.55	81.87
	MOON+ODIN	87.91	90.26	89.08	98.34	93.37	92.97	90.17	93.71
	EBO	86.15	88.58	87.36	90.59	88.39	86.85	89.60	88.86
	MOON+EBO	90.05	92.36	91.20	97.30	96.15	93.34	92.04	94.71

A.3 OOD Detection in Dense Training

In this section, to show the broad applicability of our MOON, we show our MOON can improve OOD detection in dense training. The results of baseline methods are based on the scores reported in (Yang et al., 2022).

For the model trained on CIFAR-10, we examine its OOD detection ability on two near OOD data (i.e., CIFAR-100, TIN) and four far OOD data (i.e., MNIST, SVHN, Texture, Places365). As shown in Table 11, the columns named "NearOOD" and "FarOOD" represent the average detection scores of the near OOD data and the far OOD data, respectively. We can see that our MOON provides smaller FPR-95 and larger AUROC for different near and far OOD data compared to MSP, ODIN, and EBO, where the reduction of FPR-95 can be up to 77.6% and the improvement of AUROC can be up to 27.3%. This demonstrates that our MOON can perform OOD detection more effectively compared to the original methods.

For the model trained on ImageNet-2012, we examine its OOD detection ability on four near OOD data (i.e., Species, iNaturalist, OpenImage-O, ImageNet-O) and two far OOD data (i.e., Texture, MNIST). More details about the OOD data are in Appendix B.1. As shown in Figure 8, the red and blue bars represent our MOON and MSP, respectively. We can see that our MOON provides larger AUROC and AUPR, and smaller FPR-95 almost on all of the OOD data of ImageNet-2012, showing its effective OOD detection.

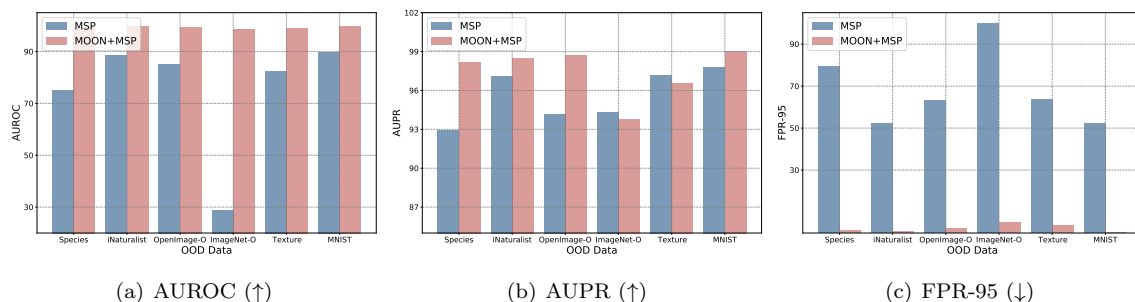


Figure 8: Comparison of OOD detection by AUROC (\uparrow), AUPR (\uparrow), and FPR-95 (\downarrow) between MOON+MSP and MSP for ImageNet-2012. Our MOON leads to larger AUROC and AUPR, and smaller FPR-95 on each OOD data of ImageNet-2012, showing its ability to improve reliability on OOD data.

Table 12: More Ablation Studies for w_f by AUROC (\uparrow) in MOON with 95% sparse ResNet-18 for CIFAR-10.

	CIFAR-100	TIN	NEAROOD	MNIST	SVHN	TEXTURE	PLACES365	FAROOD	
AUROC	$w_f = 0.1$	83.57	85.25	84.41	86.49	86.47	85.35	84.73	85.76
	$w_f = 0.5$	86.25	87.07	87.66	93.46	91.02	87.80	85.11	89.35
	$w_f = 1.0$	88.04	89.39	88.71	94.70	93.35	89.86	88.51	91.62
	$w_f = 2.0$	86.45	87.77	87.11	89.96	91.44	89.24	86.05	89.17
	$w_f = 4.0$	84.78	85.84	85.31	94.69	91.44	86.66	84.65	89.36

A.4 More Ablation Studies for w_f

We add additional ablation studies for w_f to test the sensitivity of w_f . As summarized in Appendix G, we set $w_f = 1$ for CIFAR-10. We add experiments of 95% sparse ResNet-18 with $w_f = 0.1, 0.5, 2, 4$. The AUROC results are summarized in the table below. We also include them in Appendix A.4. As shown in the Table 12, when we increase w_f from 0.1 to 4, OOD reliability first increases and then decreases after 1. While OOD reliability may be degraded when w_f is too small or too large, OOD reliability is not degraded much when w_f is between 0.5 and 2. The proper w_f value can be found with a simple hyperparameter tuning.

A.5 Additional Incremental Ablation Study

We add an incremental ablation study in which each component of the method is incremented to the previous component to better intuitively understand the utility of each component. We train 95% sparse ResNet-18 on CIFAR-10 with MOON + RigL. We find that the OOD’s reliability decreases as we gradually remove one of its components.

For MOON w/o LM, we set w_f as 0.5, 0.001, and 0.00001, respectively, to incrementally remove the loss modification component. The AUROC (%) results for MOON w/o LM are summarized in the Table 13. $w_f = 1$ refers to our MOON.

Table 13: Additional incremental ablation study for loss modification (LM) by AUROC (\uparrow) in MOON with 95% sparse ResNet-18 for CIFAR-10.

	$w_f = 1$	$w_f = 0.5$	$w_f = 0.001$	$w_f = 0.00001$
NEAROOD	88.71	86.97	86.52	85.76
FAROOD	91.62	90.18	89.41	87.76

For MOON w/o AT, we shorten T_e to 3, 2, and 1, respectively, to incrementally remove the auto tuning component. The AUROC (%) results for MOON w/o AT are summarized in the Table 14. $T_e = 5$ refers to our MOON.

Table 14: Additional incremental ablation study for auto tuning (AT) by AUROC (\uparrow) in MOON with 95% sparse ResNet-18 for CIFAR-10.

	$T_e = 5$	$T_e = 3$	$T_e = 2$	$T_e = 1$
NEAROOD	88.71	85.81	85.33	85.17
FAROOD	91.62	88.42	88.32	87.97

For MOON w/o VT, we shorten the length of epochs using the voting scheme at the end of training to 10, 5, and 2 epochs, respectively, to incrementally remove the voting scheme component. The AUROC (%) results for MOON w/o LM are summarized in the Table 15. Vote time = 20 refers to our MOON.

Table 15: Additional incremental ablation study for voting scheme (VT) by AUROC (\uparrow) in MOON with 95% sparse ResNet-18 for CIFAR-10.

	VOTE TIME = 20	VOTE TIME = 10	VOTE TIME = 5	VOTE TIME = 2
NEAROOD	88.71	85.84	85.32	84.77
FAROOD	91.62	88.16	86.78	86.76

B Appendix: Additional Details about Experiment Settings

B.1 OOD Benchmark Description

The choice of out-of-distribution (OOD) Benchmarks is according to OpenOOD (Yang et al., 2022). The distribution here refers to the "label distribution". Following the common practice of constructing OOD detection benchmarks, we treat the entire dataset as in-distribution (ID) and then gather several datasets that are not correlated with any ID category as OOD datasets. We use four OOD benchmarks, which are named after ID datasets, including MNIST (Deng, 2012), CIFAR-10 (Krizhevsky et al., 2009), CIFAR-100 (Krizhevsky et al., 2009), and ImageNet (Russakovsky et al., 2015). As mentioned by OpenOOD (Yang et al., 2022), compared to the ID dataset, the near-OOD dataset has only semantic shifts, while the far OOD further contains significant covariate (domain) shifts. The detailed description of each benchmark is as follows.

For MNIST (Deng, 2012), it is a 10-class handwriting digit dataset with 60k images for training and 10k for test. Its near-OOD datasets include NOTMNIST (Yang et al., 2021b) and FashionMNIST (Hsu et al., 2020). The far-OOD datasets include Texture (Ahmed & Courville, 2020), CIFAR-10 (Tax, 2002) and TinyImageNet (Han et al., 2022), and Places-365 (Guo et al., 2017).

For CIFAR-10 (Krizhevsky et al., 2009), it is a 10-class dataset for general object classification with 50k training images and 10k for test. Its near-OOD datasets include CIFAR-100 (Chandola et al., 2009) and TinyImageNet (Han et al., 2022), where 1,207 images are removed from TinyImageNet since they belong to CIFAR-10 classes (Yang et al., 2022). The far-OOD datasets include MNIST (Deng, 2012), SVHN (Netzer et al., 2011), Texture (Ahmed & Courville, 2020), and Places365 (Guo et al., 2017) with 1,305 images removed due to semantic overlaps.

For CIFAR-100 (Krizhevsky et al., 2009), it is a 100-class dataset for general object classification with 50k training images and 10k for test. Its near-OOD datasets include CIFAR-10 (Tax, 2002) and TinyImageNet (Han et al., 2022), where 2,502 images are removed from TinyImageNet due to the overlapping semantics with CIFAR-100 classes (Yang et al., 2022). Its far-OOD include MNIST (Deng, 2012), SVHN (Netzer et al., 2011), Texture (Ahmed & Courville, 2020), and Places365 (Guo et al., 2017) with 1,305 images removed due to semantic overlaps.

For ImageNet, it is a large-scale image classification dataset with 1000 classes. OpenOOD (Yang et al., 2022) build the OOD dataset, where they use a 10k subset of Species (Torralba et al., 2008) with 713k images, iNaturalist (Shorten & Khoshgoftaar, 2019) with 10k images, ImageNet-O (Li et al., 2021) with 2k images, and OpenImage-O (Sun et al., 2022) with 17k images as near-OOD datasets, and use Texture (Ahmed & Courville, 2020), MNIST (Deng, 2012) as far-OOD. All images belonging to the ID classes are deleted.

B.2 Computing Resources

The training and evaluation are mainly on NVIDIA Quadro RTX 6000. For CIFAR-10 and CIFAR-100, training ResNet-18 for 100 epochs with our MOON using 1 GPU takes around 1.5 hours. For ImageNet-12, training ResNet-50 for 100 epochs with our MOON using 1 GPU takes around 6 days.

C Appendix: Theoretical Analysis

In this section, we provide detailed proof of our insights in Section 4 of the main manuscript. The proof is based on Assumption C.1, which describes the characteristic of the feature space.

Assumption C.1. (Gaussian Mixture Feature Space): The feature mapping function h maps the input ID data to a Gaussian mixture $v_1\mathcal{N}(\mu_1, \Sigma_1) + v_2\mathcal{N}(\mu_2, \Sigma_2)$. Specifically, when $y = 1$, we have $h(x) \sim \mathcal{N}(\mu_1, \Sigma_1)$. And when $y = 2$, we have $f(x) \sim \mathcal{N}(\mu_2, \Sigma_2)$.

C.1 Insight 4.4: Unreliability

(Unreliability) suppose we have (x_1, y_1) from class 1 and $D_2 = \{(x, y); \|h(x) - h(x_1)\| < \epsilon, y = 2\}$ from class 2. Then, unreliability can occur around $h(x_1)$.

Proof:

The final output probability is a composition of the feature mapping function h and the softmax classification function g . As we know, the softmax function is Lipschitz continuous with a Lipschitz constant c bounded by 1.

Because of the definition of D_2 , we can know that

$$\|g(h(x)) - g(h(x_1))\| \leq c\|h(x) - h(x_1)\|. \quad (4)$$

Suppose $g(h(x_1)) = \{p_{11}, p_{12}\}$ and $g(h(x_2)) = \{p_{21}, p_{22}\}$ for any $x_2 \in D_2$. Then we can know that

$$\|p_{11} - p_{21}\| \leq c\epsilon. \quad (5)$$

Without loss of generality, suppose x_1 is predicted correctly, i.e., we have $p_{11} > 0.5$. Then, we can have

$$p_{21} \geq p_{11} - c\epsilon > 0.5, \quad \epsilon \rightarrow 0. \quad (6)$$

Then, with small ϵ , the samples in D_2 will have $p_{21} > 0.5$ and be incorrectly predicted to class 1. Thus, for any $\epsilon_0 < \epsilon$, we can define $D_2(\epsilon_0)$ and have its expected accuracy as:

$$D_2(\epsilon_0) = \{(x, y); \|h(x) - h(x_1)\| < \epsilon_0, y = 2\}, \quad (7)$$

$$\mathbf{E}_{D_2(\epsilon_0)}[1\{\hat{y} = y\}] = \mathbf{E}_{D_2(\epsilon_0)}[1\{1 = 2\}] = 0 \quad (8)$$

In this case, suppose the samples near x_1 are $D(\epsilon_0)$. And $D(\epsilon_0)$ can be divided into $D_1(\epsilon_0)$ and $D_2(\epsilon_0)$. $D_i = \{(x, y); \|h(x) - h(x_1)\| < \epsilon_0, y = i\}$. The ratio of the size of D_1 and D_2 can be approximated by

$$\frac{|D_1|}{|D_2|} = \frac{w_1}{w_2} = \frac{\mathcal{N}(h(x_1); \mu_1, \Sigma_1)}{\mathcal{N}(h(x_1); \mu_2, \Sigma_2)}, \quad \text{where } w_1 + w_2 = 1. \quad (9)$$

Then, we can calculate the unreliability level following the Definition 4.2:

$$\begin{aligned} & \mathbf{E}_{D(\epsilon)}\left[\max_{c \in \{1,2\}} \mathcal{N}(h(x); \mu_c, \Sigma_c)\right] - \mathbf{E}_{D(\epsilon)}[1\{\hat{y} = y\}] \\ &= w_1 \left(\mathbf{E}_{D_1(\epsilon)}\left[\max_{c \in \{1,2\}} \mathcal{N}(h(x); \mu_c, \Sigma_c)\right] - \mathbf{E}_{D_1(\epsilon)}[1\{\hat{y} = y\}] \right) \\ & \quad + w_2 \left(\mathbf{E}_{D_2(\epsilon)}\left[\max_{c \in \{1,2\}} \mathcal{N}(h(x); \mu_c, \Sigma_c)\right] - \mathbf{E}_{D_2(\epsilon)}[1\{\hat{y} = y\}] \right) \\ &= w_1 \left(\mathbf{E}_{D_1(\epsilon)}\left[\max_{c \in \{1,2\}} \mathcal{N}(h(x); \mu_c, \Sigma_c)\right] - 1 \right) + w_2 \left(\mathbf{E}_{D_2(\epsilon)}\left[\max_{c \in \{1,2\}} \mathcal{N}(h(x); \mu_c, \Sigma_c)\right] - 0 \right) \\ &\geq p_{11} - c\epsilon - w_1 \end{aligned} \quad (10)$$

Then, we can choose x_1 which is not very close to μ_1 such that $w_1 < p_{11} - c\epsilon - \eta$. Then, we will have:

$$\mathbf{E}_{D(\epsilon)}\left[\max_{c \in \{1,2\}} \mathcal{N}(h(x); \mu_c, \Sigma_c)\right] - \mathbf{E}_{D(\epsilon)}[1\{\hat{y} = y\}] > p_{11} - c\epsilon - w_1 > \eta. \quad (11)$$

The proof is complete.

C.2 Insight 4.6: Hard-ID Reliability

(Hard-ID Reliability) Suppose we have the same (x_1, y_1) and D_2 as in Insight 4.4. If the model is trained with our MOON method and the extra dimension successfully stores the unknown information, the unreliability can be solved, i.e.,

$$\mathbf{E}_{D(\epsilon)}[\max_{c \in \{1,2\}} \mathcal{N}(h(x); \mu_c, \Sigma_c)] - \mathbf{E}_{D(\epsilon)}[1\{\hat{y} = y\}] < \eta. \quad (12)$$

Proof:

Following the notations in the proof of Insight 4.4, we can know that unreliability around x_1 has two parts. One is from D_1 and the other is from D_2 . And the majority of the unreliability comes from D_2 . Thus, in order to reduce the discrepancy between confidence and accuracy, we need to mainly reduce the part of D_2 , which is:

$$\mathbf{E}_{D_2(\epsilon)}[\max_{c \in \{1,2\}} \mathcal{N}(h(x); \mu_c, \Sigma_c)] - \mathbf{E}_{D_2(\epsilon)}[1\{\hat{y} = y\}] \quad (13)$$

Suppose the two classes of data are balanced. Since x_1 is predicted correctly, we can know that $w_1 > w_2$ and $|D_1| > |D_2|$.

In this case, if the model can find a better feature mapping h that does not have such a discrepancy for any set of data D , then there is no safety problem. However, if finding such a suitable feature mapping h is too difficult, which is usually the case, we can only change the softmax classification function g . In sparse training, the update route is cut off, generating spurious local optimization, leading to a more challenging exploration of the weight space and thus an inability to find a suitable feature mapping h .

If we choose the widely-used cross entropy loss L which in our case will take the form as below:

$$\begin{aligned} L(D) &= L(D_1) + L(D_2) \\ &= - \sum_{i \in D_1} \log p_{i1} - \sum_{i \in D_2} \log p_{i2} \\ &= - \sum_{i \in D_1} \log p_{i1} - \sum_{i \in D_2} \log(1 - p_{i1}) \end{aligned} \quad (14)$$

Since it is difficult to find a better mapping h , we assume h is fixed in this case. If ϵ is small, then the gradient of samples in $D(\epsilon)$ will be similar to that of x_1 . Suppose $g(h(x_1)) = (p_1^*, p_2^*)$. Then, we can have:

$$L(D) = - \sum_{i \in D_1} \log p_{i1} - \sum_{i \in D_2} \log(1 - p_{i1}) \quad (15)$$

$$\approx -|D_1| \log p_1^* - |D_2| \log(1 - p_1^*) \quad (16)$$

And the gradient of loss will be:

$$\nabla L(D) \propto \frac{(|D_2| + |D_1|) * p_1^* - |D_1|}{p_1^*(1 - p_1^*)} \quad (17)$$

Thus, to reduce the loss, p_1^* will stuck at $\frac{|D_1|}{|D_1| + |D_2|}$ and can not reduce the discrepancy, implying severe unreliability in D .

If we choose our MOON, there will be three dimensions in the output probability and $g(h(x_1)) = (p_1^*, p_2^*, p_3^*)$. And the new loss will take the form as below:

$$\begin{aligned} L(D) &= L(D_1) + L(D_2) \\ &= - \sum_{i \in D_1} \log p_{i1} - \sum_{i \in D_2} \left(1 + \frac{w}{1 + wp_{i3}}\right) \log p_{i2} \\ &= - \sum_{i \in D_1} \log p_{i1} - \sum_{i \in D_2} \left(1 + \frac{w}{1 + wp_{i3}}\right) \log(1 - p_{i1}) \\ &\approx -|D_1| \log p_1^* - |D_2| \left(1 + \frac{w}{1 + wp_3^*}\right) \log(1 - p_1^*) \end{aligned} \quad (18)$$

Then, the gradient of the loss will be as below

$$\nabla L(D) \propto \frac{(|D_1| + |D_2| + \frac{w}{1+wp_3^*}|D_2|) * p_1^* - |D_1|}{p_1^*(1-p_1^*)} \quad (19)$$

We can see that in order to minimize the loss, we can update not only p_1^* but also p_3^* , thus providing more degrees of freedom for the model to learn reliable predictions. Instead of increasing p_1^* and being stuck in an unreliable state, the model can increase p_3^* when it encounters hard-ID samples. Suppose we have nonzero p_3^* after the parameter update. We can calculate the new unreliability level following the Definition 4.2:

$$\begin{aligned} & \mathbf{E}_{D(\epsilon)}[\max_{c \in \{1,2\}} \mathcal{N}(h(x); \mu_c, \Sigma_c)] - \mathbf{E}_{D(\epsilon)}[1\{\hat{y} = y\}] \\ &= w_1 \left(\mathbf{E}_{D_1(\epsilon)}[\max_{c \in \{1,2\}} \mathcal{N}(h(x); \mu_c, \Sigma_c)] - \mathbf{E}_{D_1(\epsilon)}[1\{\hat{y} = y\}] \right) \\ & \quad + w_2 \left(\mathbf{E}_{D_2(\epsilon)}[\max_{c \in \{1,2\}} \mathcal{N}(h(x); \mu_c, \Sigma_c)] - \mathbf{E}_{D_2(\epsilon)}[1\{\hat{y} = y\}] \right) \\ &= w_1 \left(\mathbf{E}_{D_1(\epsilon)}[\max_{c \in \{1,2\}} \mathcal{N}(h(x); \mu_c, \Sigma_c)] - 1 \right) + w_2 \left(\mathbf{E}_{D_2(\epsilon)}[\max_{c \in \{1,2\}} \mathcal{N}(h(x); \mu_c, \Sigma_c)] - 0 \right) \\ &\leq w_1(p_{11} + c\epsilon - p_3^* - 1) + w_2(p_{11} + c\epsilon - p_3^*) \\ &= p_{11} + c\epsilon - p_3^* - w_1 \end{aligned} \quad (20)$$

Since the extra dimension (i.e., p_3^*) successfully stores the unknown information, we can assume that p_3^* is reasonably large, i.e., $p_3^* > p_{11} + c\epsilon - w_1 - \eta$. Then, the unreliability level can be reduced to a value less than η :

$$\mathbf{E}_{D(\epsilon)}[\max_{c \in \{1,2\}} \mathcal{N}(h(x); \mu_c, \Sigma_c)] - \mathbf{E}_{D(\epsilon)}[1\{\hat{y} = y\}] \leq p_{11} + c\epsilon - p_3^* - w_1 < \eta \quad (21)$$

The proof is complete.

C.3 Insight 4.8: OOD Reliability

(OOD Reliability) Suppose we achieve Hard-ID Reliability in Insight 4.8 with our MOON method, we can have lower confidence on OOD data, implying stronger OOD detection.

Proof:

We know that hard-to-detect OOD data D_3 usually have features close to those of hard ID data D_2 , which is similar to the scenario described in Insight 4.4. Otherwise, if the features of the hard-to-detect OOD data are very different from those of hard ID data, then the OOD data becomes easy to detect without the OOD unreliability.

Thus, these hard-to-detect ID samples can be viewed as pseudo-OOD data. And the $\{h(x_2); x_2 \in D_2\}$ are close to $\{h(x_3); x_3 \in D_3\}$. Then we can follow the proof of Insight 4.6 and show that:

$$\mathbf{E}_{D_3(\epsilon)}[\max_{c \in \{1,2\}} \mathcal{N}(h(x); \mu_c, \Sigma_c)] \text{ is reduced.} \quad (22)$$

In this way, we are able to have smaller confidence in the hard-to-detect OOD data D_3 , which helps to enhance the OOD reliability. This describes how we can extract unknown information from hard ID data, explaining the outlier-exposure-free property of MOON.

D Appendix: Limitations of Our MOON

D.1 More General Reliability

Despite the enhanced OOD reliability achieved in sparse training, MOON does not address this matter comprehensively from a broader reliability perspective, including robust generalization (Silva & Najafirad,

2020; Özdenizci & Legenstein, 2021; Chen et al., 2022a) and adaptation (Emam et al., 2021; Alayrac et al., 2022; Hu et al., 2022), which are equally vital aspects of reliability and deserve further investigation (Tran et al., 2022).

D.2 Reliability in Large Generative Models

Additionally, the effectiveness of MOON remains unexplored in the context of widely employed large generative models (Ouyang et al., 2022; Croitoru et al., 2023). On the one hand, as model size expands, novel changes in model characteristics may arise (Wei et al., 2022b). On the other hand, given the prevalence of non-classification tasks within LLMs, the exploration of how to evaluate their reliability remains an uncharted domain.

E Broader Impact

This work is likely to encourage other future work on more general reliability in sparse training to achieve efficiency and comprehensive reliability in real-world DNN deployments.

In addition, as large generative models develop, both computational efficiency and decision reliability are important aspects of their application. This work can increase the progress of efficient and reliable large generative models.

F FLOPs Analysis

In this section, we add FLOPs analysis to MOON. We use 80% sparse ResNet-50 on Image-Net-2012 as an example. The training FLOPs using RigL are about $7.4e17$ (Evci et al., 2020). For our MOON, the increased FLOPs come from three components, i.e., loss modification, auto tuning, and voting scheme.

(i) For loss modification and auto-tuning.

- In the early stage where $w = 0$, we have about $1.3e5$ FLOPs in each iteration because of the computation of β .
- After the early stage, from the calculation of w and the new loss, we have about $2.6e5$ FLOPs in each iteration.
- Thus, the loss modification and auto tuning introduce an additional $2.3e15$ FLOPs.

(ii) For voting scheme,

We start doing weight averaging in 80% of the training epoch and have about $1.8e9$ FLOPs from the weight averaging. In each epoch after the 80% training epoch, we also have about $2.4e15$ FLOPs from the batchNorm buffer updates. Thus, the voting scheme introduces an additional $4.8e16$ FLOPs.

Overall, our MOON introduces an additional $5.0e16$ FLOPs, which is about 6.8% of the original RigL’s FLOPs. The main cause of the increase in FLOPs is the update of the batchNorm buffer. To further reduce the increase of FLOPs, we can reduce the update frequency of the batchNorm buffer.

We also conduct experiments to compare the training time using our MOON and baseline methods. We train 80%, 90%, 95%, and 99% sparse ResNet-18 on both CIFAR-10 and CIFAR-100 using MOON + RigL and RigL. We denote the training time of our benchmark method, RigL, as 1 to help understand exactly what overhead our MOON adds to the training process. The results are summarized in the Table 16-17. We can see that MOON adds less than 5% overhead.

Table 16: Training time comparison using our MOON + RigL and RigL with 80%, 90%, 95%, and 99% sparse ResNet-18 on both CIFAR-10.

	CIFAR-10 (80%)	CIFAR-10 (90%)	CIFAR-10 (95%)	CIFAR-10 (99%)
RigL	1	1	1	1
MOON + RigL	1.045	1.042	1.039	1.046

Table 17: Training time comparison using our MOON + RigL and RigL with 80%, 90%, 95%, and 99% sparse ResNet-18 on both CIFAR-100.

	CIFAR-10 (80%)	CIFAR-10 (90%)	CIFAR-10 (95%)	CIFAR-10 (99%)
RigL	1	1	1	1
MOON + RigL	1.049	1.046	1.048	1.043

G Hyperparameter Tuning

The hyperparameters of the baseline method follow their original settings in (Evci et al., 2020; Yang et al., 2022). The hyperparameters of our MOON are described as follows.

(i) For the learning rate, following (Yang et al., 2022), we use the cosine annealing scheduler, where the maximum learning rate is set to 1.2 and the minimum learning rate is set to 0.08.

(ii) For the fraction of weights removed and added (pruning ratio) in each sparse pattern update, we follow the original settings in (Evci et al., 2020; Sundar & Dwaraknath, 2021).

- The initial fraction is 0.3.
- This fraction decays in the mask update step by cosine annealing.
- The score is set to zero after 70% of the training cycles.

(iii) For the weight distribution, we follow the original settings in (Evci et al., 2020; Sundar & Dwaraknath, 2021) and initialize the mask by Erdos-Renyi-Kernel (ERK).

(iv) For w_f and r

- For MNIST, we set w_f and r as 0.01 and 64, respectively.
- For CIFAR-10, we set w_f and r as 1 and 64, respectively.
- For CIFAR-100, we set w_f and r as 2 and 64, respectively.
- For ImageNet-2012, we set w_f and r as 0.001 and 64, respectively.

H Feature Visualization

One of the assumptions on which our theory is based is that the feature distribution of a DNN feature extractor is a Gaussian mixture. Additional experiments are added to support this assumption. Specifically, we train ResNet-18 on CIFAR-10 with 80%, 90%, 95% and 99% sparsity and collect features before the last layer. Then, to visualize the feature distribution, we use the PCA method to reduce the dimensionality and plot the histogram of the first component.

As shown in Figure 9-12, the feature distribution shows a high density in the center and then decreases towards the two sides across all classes and sparsity levels. This characterization is consistent with a Gaussian distribution. Therefore, the overall distribution for all classes can be approximated by a Gaussian mixture distribution, supporting our assumption.

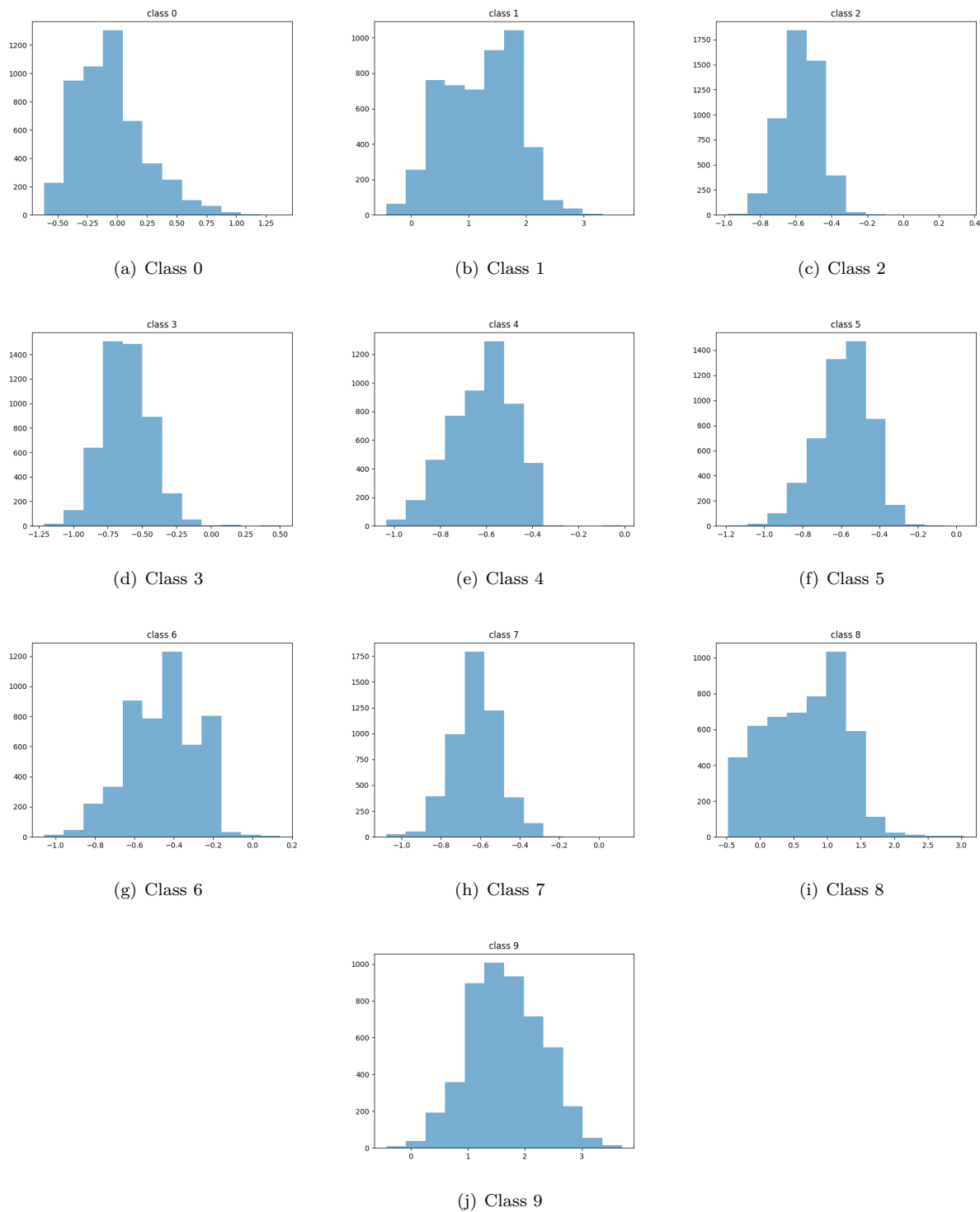


Figure 9: Feature distribution visualization on CIFAR-10 for 80% sparse ResNet-18. The feature distribution shows a high density in the center and then decreases towards the two sides across all classes.

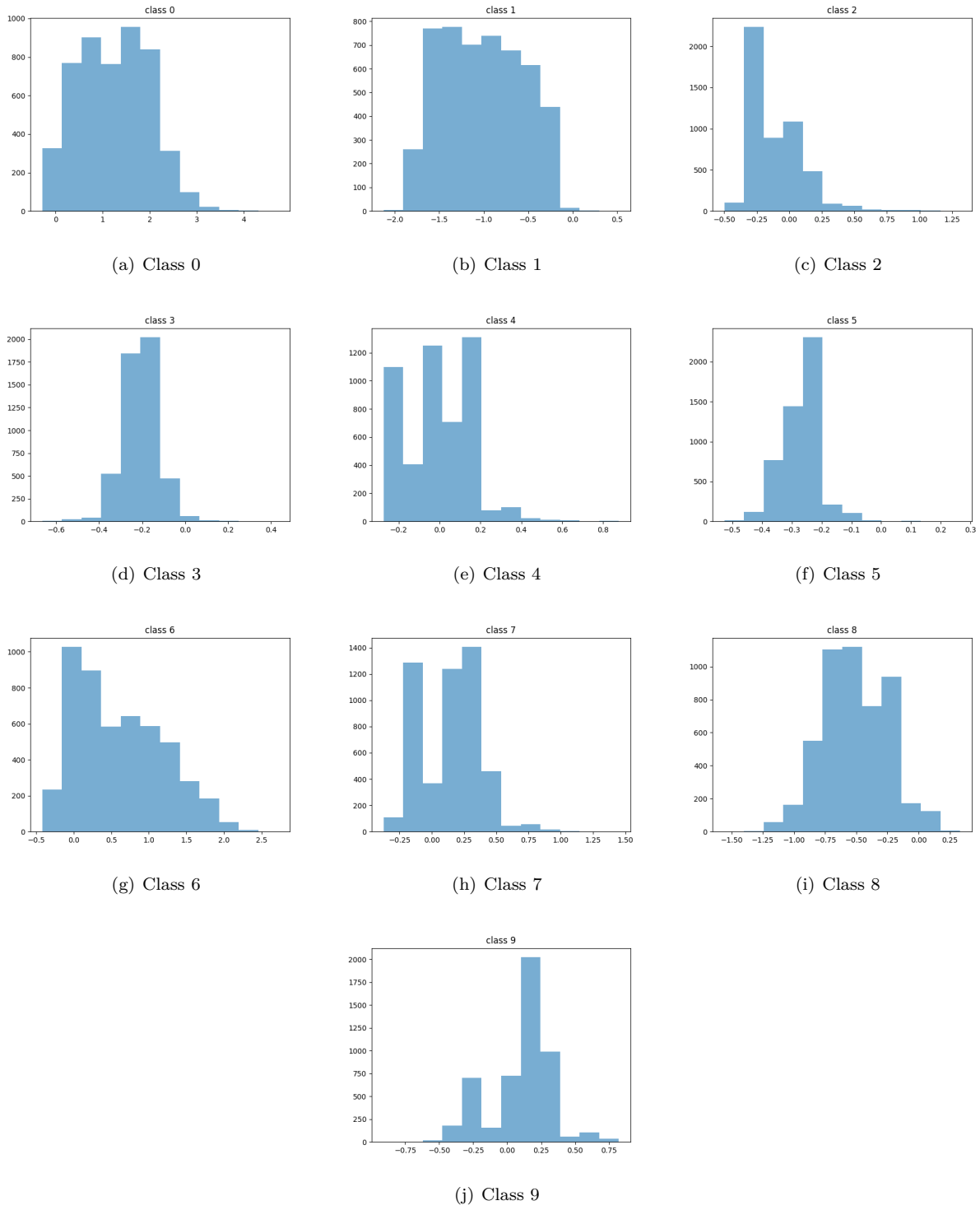


Figure 10: Feature distribution visualization on CIFAR-10 for 90% sparse ResNet-18. The feature distribution shows a high density in the center and then decreases towards the two sides across all classes.

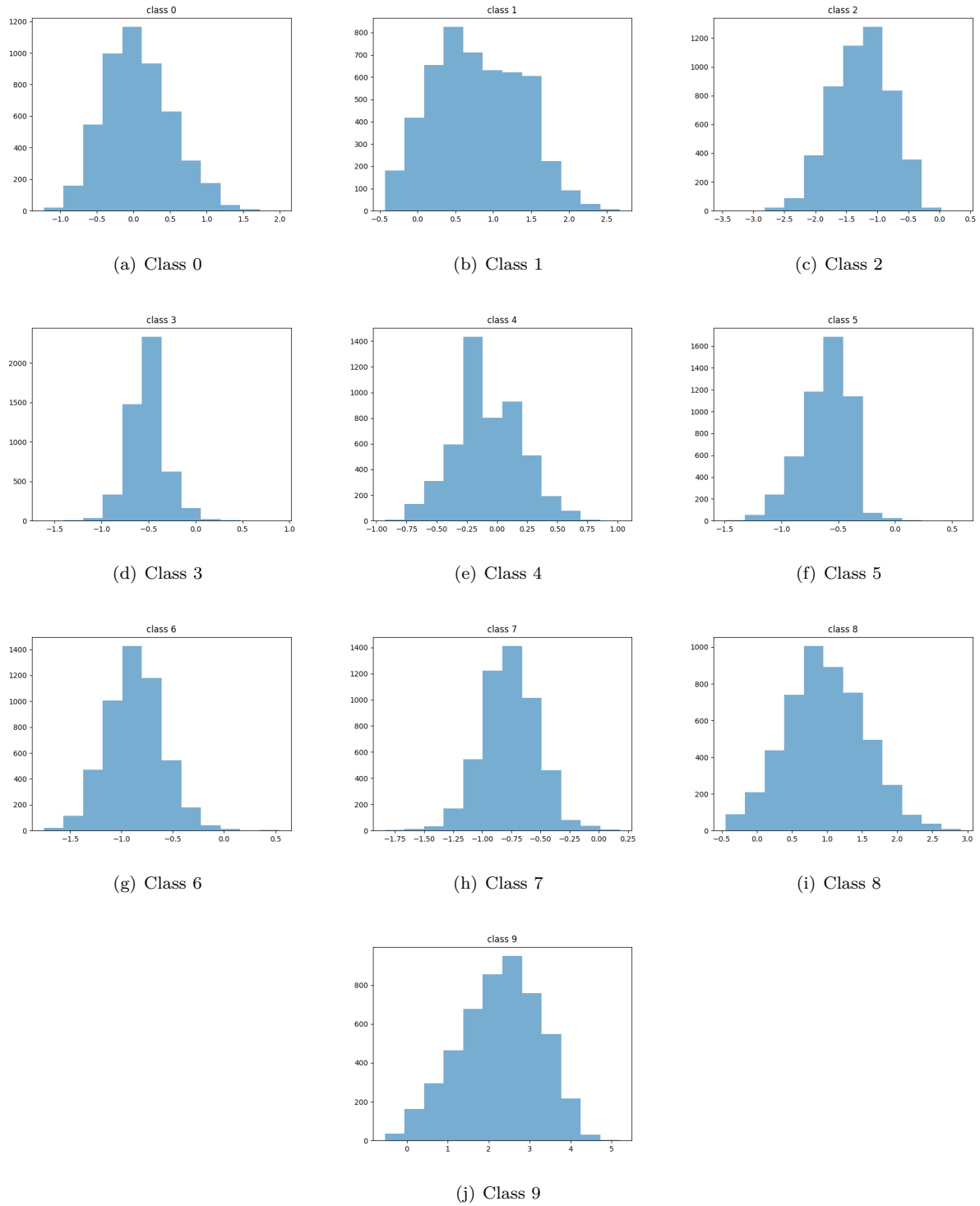


Figure 11: Feature distribution visualization on CIFAR-10 for 95% sparse ResNet-18. The feature distribution shows a high density in the center and then decreases towards the two sides across all classes.

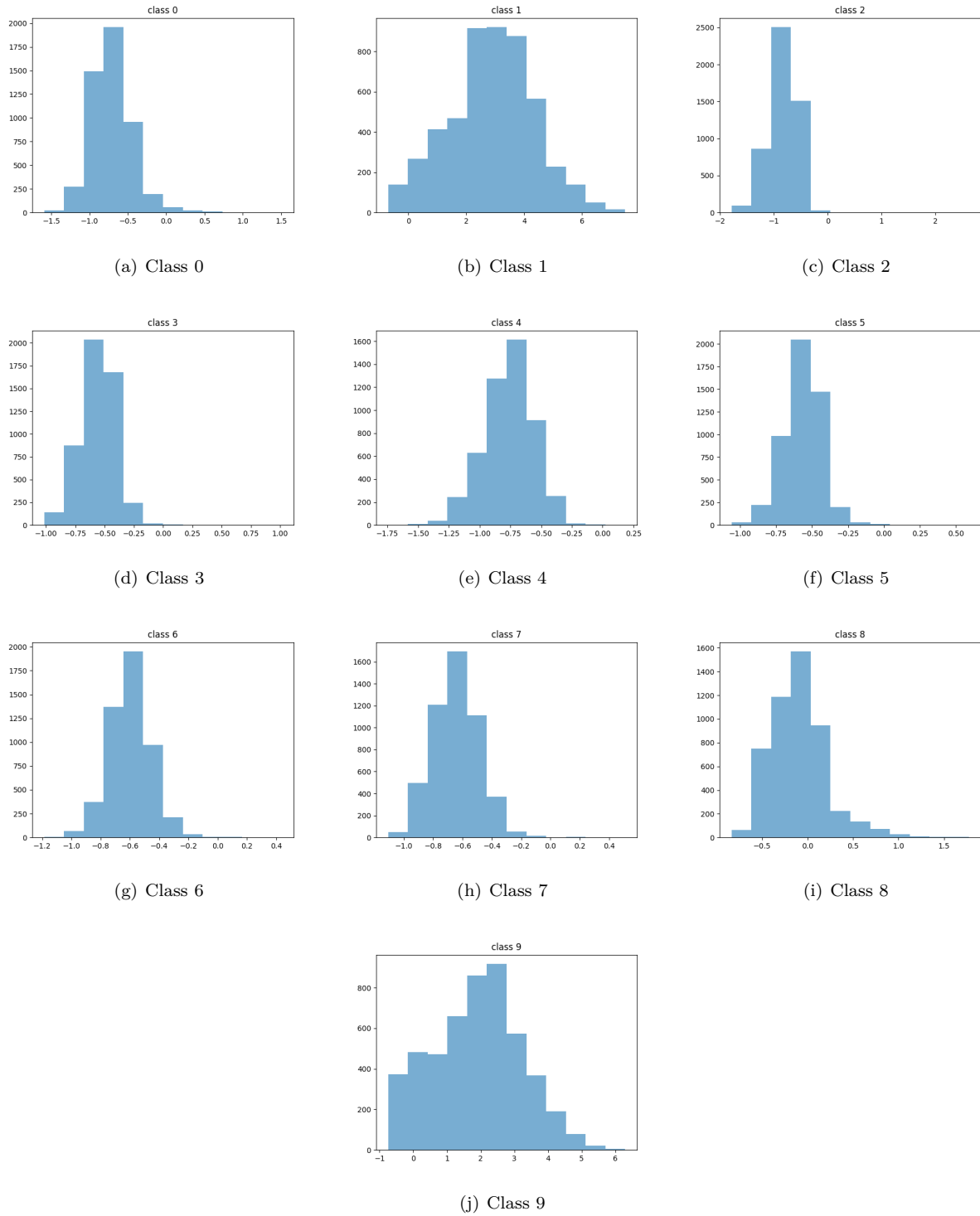


Figure 12: Feature distribution visualization on CIFAR-10 for 99% sparse ResNet-18. The feature distribution shows a high density in the center and then decreases towards the two sides across all classes.